Conditions. A Grand Canonical Monte Carlo Simulation Study

Réka A. Horváth[a], György Hantal[b], Sylvain Picaud[c], Milán Szőri[d], Pál Jedlovszky[e,*]

[a]*Apáczai Csere János School of the ELTE University, Papnövelde u. 4. H-1053 Budapest, Hungary*

[b]*Faculty of Physics, University of Vienna, Boltzmanngasse 5, A-1090 Vienna, Austria*

[c]*Institut UTINAM (CNRS UMR 6213), Université Bourgogne Franche-Comté, 16 route de Gray, F-25030 Besançon, France*

[d]*Institute of Chemistry, University of Miskolc, Egyetemváros A/2, H-3515 Miskolc, Hungary*

[e]*Department of Chemistry, Eszterházy Károly University, Leányka u. 6, H-3300 Eger, Hungary*

Running title: Adsorption of methylamine on ice

*E-mail: jedlovszky.pal@uni-eszterhazy.hu

Abstract:

The adsorption of methylamine at the surface of amorphous ice is studied at various temperatures, ranging from 20 K to 200 K, by grand canonical Monte Carlo simulations under conditions that are characteristic to the interstellar medium (ISM). The results are also compared with those obtained earlier on crystalline (I_h) ice. We found that methylamine has a strong ability of being adsorbed on amorphous ice, involving also multilayer adsorption. The decrease of the temperature leads to a substantial increase of this adsorption ability, thus, considerable adsorption is seen at 20-50 K even at bulk gas phase concentrations that are comparable with that of the ISM. Further, methylamine molecules can also be dissolved in the bulk amorphous ice phase. Both the adsorption capacity of amorphous ice and the strength of the adsorption on it are found to be clearly larger than those corresponding to crystalline (I_h) ice, due to the molecular scale roughness of the amorphous ice surface as well as to the lack of clear orientational preferences of the water molecules at this surface. Thus, the surface density of the saturated adsorption monolayer is estimated to be 12.6 ± 0.4 μmol/m^2, 20% larger than the value of 10.35 μmol/m^2, obtained earlier for I_h ice, and at low enough surface coverages the adsorbed methylamine molecules are found to easily form up to three hydrogen bonds with the surface water molecules. The estimated heat of adsorption at infinitely low surface coverage is calculated to be -69 ± 5 kJ/mol, being rather close to the estimated heat of solvation in the bulk amorphous ice phase of -74 ± 7 kJ/mol, indicating that there are at least a few positions at the surface where the adsorbed methylamine molecules experience a bulk-like local environment.

1. Introduction

The origin and formation of amino acids are of particular interest in astrochemical research, because their presence in the interstellar medium (ISM) may provide clues to the delivery of prebiotic molecules to the early Earth, the possible origins of life on Earth,[1-3] and the possibility of Earth-like life elsewhere in the Universe.[4] Glycine and methylamine (CH_3NH_2) are not just simple structural analogs (related to each other by the presence or absence of the carboxyl group), but methylamine is also proposed to be a precursor of glycine. In the interstellar medium, CH_3NH_2 can be formed either by CH_4 and NH_3, well known to be abundant in the ISM, under cosmic ray irradiation,[5,6] or by the hydrogenation reaction of HCN on icy dust surfaces. CH_3NH_2 molecules that are trapped at solid surfaces can then thermally react with CO_2 to form carbamate, which can be converted to a glycine salt under vacuum ultraviolet irradiation.[7] Alternative pathways of this reaction, occurring through the CH_2NH_2 radical[8,9] or acetic acid[10] were also proposed in the literature.

Both glycine and methylamine compounds are common in the terrestrial biosphere,[1] and both have also been detected in comet-exposed material from the *Stardust* sample return mission to comet Wild 2,[11] by the Cometary Sampling and Composition (COSAC) instrument onboard the *Rosetta Philae* mission,[12] as well as in multiple extraterrestrial samples, including carbonaceous chondrites.[13-15] Carbonaceous chondrites, notably the CI (e.g. Orgueil) and CM (e.g. Murchinson) groups, contain high percentages (3% to 22%) of water,[16] and also methylamine in the concentration of 331 nmol/g (Orgueil) and 85 nmol/g (Murchison).[17] Generally, interstellar[18] and cometary[19] dust grains are frequently covered by amorphous solid water, this mantle also traps volatile reactants, and the water molecule can act both as a catalyst and as a chemical reactant.[20] In order to characterize methylamine astrochemistry, Vinogradoff et al. reported a laboratory experiment, in which methylamine and formaldehyde were found to quickly react at interstellar or cometary ice analogues at astronomically relevant temperatures with a measured activation energy of 1.1 ± 0.05 kJ/mol.[21] However, in the absence of relevant experiments, desorption behavior of methylamine from the ice surface was estimated to be identical with that of ammonia (with a value of 3×10^{12} s as the pre-exponential factor, and 25 kJ/mol as the activation energy).[21] As this example also shows, a major stumbling-block in our understanding of prebiotic chemistry in the ISM is the lack of a standardized and comprehensive approach to simulate grain-surface chemistry.[22] Furthermore, improved gas-

grain astrochemical models need to be developed in order to interpret the high-resolution data provided by Atacama Large Millimeter Array (ALMA).

Besides laboratory experiments, molecular details of the adsorption of methylamine at icy surfaces can also be investigated by computer simulation methods, in order to improve the current adsorption models used in astrochemistry. Such methods can well complement experiments, as they can provide a full, three-dimensional insight of atomistic resolution into the system of interest.[23] Among the various computer simulation techniques, the grand canonical Monte Carlo (GCMC) method[23,24] is particularly suitable for studying adsorption, since here the chemical potential rather than the number of the adsorbate molecules in the basic box is fixed, and thus, by systematically varying the chemical potential and determining the number of adsorbate molecules in a set of simulations, the adsorption isotherm can be determined, and simulation results can be analyzed in detail at surface coverage values that are relevant for the given adsorption process. The GCMC method has been successfully applied in the past two decades for a set of systems, such as for the adsorption of various small molecules at carbonaceous surfaces,[25-31] metal oxides,[32-35] covalent organic frameworks,[36-38] crystalline ice,[39-48] water clathrates,[49] kaolinite,[50,51] zeolites,[52-58] self-assembled monolayers,[59,60] and protein crystals.[61]

Since icy surfaces in the interstellar medium are predominantly covered by low density amorphous ice (LDA),[18,19] here we study the adsorption of methylamine at the surface of LDA ice by GCMC simulations at temperatures that are relevant to the interstellar medium (i.e., a few tens of K). Besides its potential role in prebiotic evolution, methylamine, released primarily by decaying bodies,[62] is also an abundant atmospheric pollutant, being involved in the catalytic ozone destruction process occurring at the polar stratospheres[63] as well as increasing aerosol nucleation rates in the lower troposphere.[64] For this purpose, recently we performed a detailed GCMC analysis of the adsorption of methylamine at the surface of crystalline, I_h ice at the tropospheric temperature of 200 K. Thus, the present study provides also an excellent opportunity to investigate in detail the role of the state of the adsorbing phase (i.e., crystalline vs. amorphous ice) as well as that of the temperature in the details of the adsorption process. For this purpose, here we determine the adsorption isotherm of methylamine at the surface of LDA ice, and analyze in detail the properties of the adsorption layer at the temperatures of 200 K, 150 K, 100 K, 50 K, and 20 K, corresponding to the adsorption in the colder parts of the interstellar medium. Further, the comparison of the results

obtained at 200 K with our earlier data obtained at the surface of I$_h$ ice[47] provides information on how the properties of the adsorption layer depends on the structure of the adsorbing phase, whereas the comparison of the results obtained at different temperatures can shed light on the temperature dependence of the adsorption process, and even allows us to extrapolate to lower temperatures, at which computer simulation studies cannot be done within reasonable time.

The paper is organized as follows. In sec. 2 details of the performed calculations, including GCMC simulations and ITIM analysis, are given. The results concerning the adsorption isotherm, the building up of the subsequent molecular layers of the adsorbate as well as the orientation and energetics of the adsorbed methylamine molecules that are in direct contact with the ice phase are discussed in detail in sec. 3. Finally, in sec. 4 the main conclusions of this study are summarized.

2. Computational Details

2.1. Grand Canonical Monte Carlo Simulations. The adsorption of methylamine at the surface of low density amorphous ice has been simulated, using the Monte Carlo method, on the grand canonical (μ,V,T) ensemble at the temperatures (T) of 200 K, 150 K, 100 K, 50 K, and 20 K. The X, Y, and Z edges of the rectangular basic simulation box have been 100 Å, 35.926 Å, and 38.891 Å, respectively, X being the axis perpendicular to the ice surface. The basic box has consisted of 2880 water molecules. At each temperature, simulations have been performed at several chemical potentials of methylamine, ranging from values corresponding to practically no methylamine molecules in the basic box to those corresponding to the condensed phase of methylamine. The chemical potential values at which the simulations have been performed at the various temperatures, as well as the mean number of the methylamine molecules present in the basic box, resulted from these simulations, are summarized in Tables S1-S5 of the supporting information.

To be consistent with our previous study concerning I$_h$ ice,[47] water and methylamine molecules have been described by the TIP5P model[65] and the potential model proposed by Impey et al.,[66] respectively. TIP5P is known to be one of the best water models in describing low temperature aqueous phases,[67] as it reproduce very well, among others, the temperature of maximum density[65,67] as well as the melting point[67] of water. Further, TIP5P reproduces the LDA/HDA liquid-liquid phase transition of water in the temperature range considered here.[68]

Both of these models used are rigid and pairwise additive, i.e., the total potential energy of the system is assumed to be the sum of the contributions of all molecule pairs. The interaction energy of a molecule pair consists of the Lennard-Jones and charge-charge Coulomb contributions of all the respective pairs of interaction sites. The CH_3 group of the methylamine molecule is treated as a single interaction site (united atom), whereas the water model has two non-atomic interaction sites, marked by L, located at the positions of the two lone pairs of the O atom. The interaction of a molecule pair is truncated to zero beyond the center-center cut-off distance of 12.5 Å. The interaction and geometry parameters of the potential models used are collected in Tables 2 and 3 of Ref. 47, respectively.

The simulations have been performed using the program MMC[69] in the same way as described in our earlier paper.[47] Thus, in every Monte Carlo step either, by 50% probability, a randomly chosen molecule has been randomly translated by no more than 0.25 Å and randomly rotated by no more than 15°, or by 50% probability, the number of the methylamine molecules in the basic box has been attempted to be changed by inserting or removing a molecule. Water and methylamine molecules have been selected for particle displacement steps with equal probabilities, and methylamine insertions and deletions have also been performed with 50%-50% probabilities. The insertion/deletion attempts have been made using the cavity biased scheme of Mezei,[70,71] thus, insertions have only been attempted into centers of empty cavities of the radius of at least 2.6 Å. Suitable cavities have been searched for along a 100×100×100 grid, which has been regenerated after every 10^6 Monte Carlo steps. Particle displacement and insertion/deletion attempts have been accepted or rejected according to the standard Metropolis algorithm,[23,72] and according to the acceptance criterion of the cavity biased scheme,[70,71] respectively.

To create the LDA ice phase and surface, we started from the crystalline I_h ice phase used in our previous work. This phase was melted by thermalizing it, on the canonical (N,V,T) ensemble, at 350 K by performing 3×10^8 Monte Carlo steps, followed by another 10^8 Monte Carlo steps at 300 K. The melted system was then quenched by setting the temperature to 200 K, and performing another 10^8 Monte Carlo steps. Then two methylamine molecules were added to the vapor phase of the system, and this configuration has been used as the starting point of all grand canonical ensemble simulations. The system has then been equilibrated at every temperature and chemical potential by performing $10^9 – 3\times10^9$ Monte Carlo steps, until neither the average total energy of the system nor the mean number of methylamine molecules

have shown even traces of a systematic drift. The mean number of the methylamine molecules has then been determined in every case by generating a 2×10^8 Monte Carlo steps long equilibrium trajectory. Equilibrium snapshots of the 20 K system are shown in Figure 1, both in top and side views, as obtained at four different chemical potential values of methylamine.

To investigate the properties of the adsorption layer in detail, at selected chemical potential values, 5000 equilibrium sample configurations, separated by 4×10^5 Monte Carlo steps long runs each, have been saved from the 2×10^9 Monte Carlo steps long production runs for further evaluation. At each temperature four such chemical potential values have been chosen. The first of these values always corresponds to the presence of only very few, isolated methylamine molecules at the ice surface, the second one to a partly unsaturated monolayer, in which the methylamine molecules are no longer isolated from each other, the third one to a more or less saturated monolayer, while the fourth one to multilayer adsorption. For comparison with our earlier results, at 200 K dumping of configurations has also been done at two more chemical potential values, at which detailed analysis of the adsorption layer on I_h ice was earlier performed.[47] Finally, for reference purposes, configurations have also been saved for analyses at a μ value corresponding to the condensed phase of methylamine at 200 K. These μ values, together with the mean number of methylamine molecules resulted from the corresponding simulations, are collected in Table 1, and are also indicated in Tables S1-S5 of the supporting information.

2.2. Identification of the Dissolved and First Layer Methylamine Molecules. It has turned out from the simulations that, unlike in the case of crystalline I_h ice, methylamine molecules are not only adsorbed at the surface of the amorphous LDA ice, but they are also incorporated in the bulk ice phase, as seen also in some of the snapshots of Fig. 1. This finding is in a clear accordance with the results of the experiments of Vinogradoff et al., performed on methylamine/water mixtures under astrochemical conditions.[21] Further, the surface of the amorphous ice phase, unlike that of the crystalline ice phase used in our previous simulation, [47] is corrugated on the molecular length scale. Therefore, the first molecular layer of the adsorbed phase of methylamine (i.e., the methylamine molecules that are in a direct contact with the ice phase) cannot simply be identified in the conventional way, with the first peak of the methylamine density profile. Instead, first layer methylamine molecules have to be identified

with an intrinsic surface analyzing method.[73] Further, the methylamine molecules forming the first layer are needed to be distinguished not only from those belonging to one of the subsequent molecular layers in the adsorbed phase, but also from the ones that are dissolved into the bulk amorphous ice phase.

To perform the identification of the methylamine molecules forming the first adsorbed molecular layer as well as those inserted into the amorphous ice phase, we have applied a modified version of the Identification of Truly Interfacial Molecules (ITIM) method, developed originally to identify the instantaneous surface of fluid phases in computer simulations.[74] This complex goal has been achieved in two major steps. In the first one, the ITIM algorithm has been performed solely on the ice phase, to identify the molecularly corrugated boundaries of the adsorbent. As a result, every methylamine molecule residing between these boundaries can be considered as being dissolved in the ice phase, and hence can be excluded from further analyses. This first round of the ITIM analysis has been followed by a second one, this time performed "inside-out" on the remaining methylamine molecules, to identify the innermost adsorbates in the immediate vicinity of the ice surface. This set of interface methylamine molecules has been considered as the first adsorbed layer in all subsequent analyses. In the ITIM procedure, probe spheres of a radius of 2 Å have been moved perpendicular to the plane of the macroscopic interface until they "touched" the outmost atom of the phase to be analyzed. Probes were "launched" from a grid set up above the surface. The spacing of the grid was set to 0.5 Å. The choice of these parameters was previously found to ensure an optimal sampling for molecularly corrugated surfaces.[73,74] This method is illustrated in Fig. 1, where methylamine molecules belonging to the first molecular layer of the adsorbed phase are shown by yellow, those being in the outer part of the adsorption layer by cyan, while those inserted into the ice phase by dark blue color.

3. Results and Discussion

3.1. Adsorption Isotherm and Density Profiles. The average number of methylamine molecules present in the basic simulation box, $<N>$, is shown as a function of the chemical potential in Figure 2 as obtained from our GCMC simulations at the five temperatures considered. The chemical potential values at which sample configurations have been saved for detailed analyses are also indicated in the figure. It should be noted that the value of $<N>$ has

been calculated on-the-fly, whereas, due to its computational cost, the ITIM procedure described in sec. 2 can only be performed, and hence also the distinction between the adsorbed and dissolved methylamine molecules can only be made on saved sample configurations. Therefore, the isotherms shown in Fig. 2 include both the adsorbed and dissolved methylamine molecules. The isotherms corresponding to different temperatures are rather similar to each other in shape: they all rise sharply and continuously up to the sudden jump corresponding to the point of condensation, without exhibiting any marked plateau. The very steep rise of the isotherms, occurring immediately before condensation, suggests that the adsorption of methylamine is not limited to one single molecular layer. As expected, the isotherms are shifted to higher chemical potential values with decreasing temperature. The μ values corresponding to the point of condensation, denoted here as μ_0, are estimated from the position of the steepest rising part of the isotherms to be -26.26, -27.76, -30.20, -32.34, and -33.66 kJ/mol at 20, 50, 100, 150, and 200 K, respectively. As is seen from Figure 3, the value of μ_0 increases practically linearly with decreasing temperature. Considering that, for one component, μ is simply the molar free energy, and hence the molar entropy, S^m, is related to its temperature derivative as $S^m = -(\partial\mu/\partial T)$, the observed linear temperature dependence of μ_0 implies that the corresponding molar entropy is constant (i.e., 41.9 ± 2.7 J/mol K).

The comparison of the isotherms obtained at 200 K at the surfaces of crystalline, I_h[47] and amorphous ice is shown in the inset of Fig. 2. As is seen, there are several important differences between the two isotherms. First, at low μ values, i.e., below about -40 kJ/mol, the isotherm corresponding to amorphous ice goes consistently above that of the I_h ice. Since in this chemical potential range even the first molecular layer of methylamine is far from being saturated, this difference indicates stronger interaction of the methylamine molecules with the corrugated surface of amorphous ice, containing several troughs on the molecular length scale within which an adsorbed molecule can have more contact with the surrounding waters, than with the flat surface of I_h ice. Second, the clear plateau of the isotherm corresponding to I_h ice in the μ range between about -40 and -35 kJ/mol, corresponding to the saturated monolayer, is completely missing in the case of amorphous ice. Instead, this latter isotherm rises continuously even in this μ range, indicating the building up of outer molecular layers of methylamine here. The lack of particular stability of the saturated monolayer at the amorphous ice surface is probably due to the fact that the adsorbed monolayer reflects the corrugation of

the ice surface, and hence it also has several pockets of negative local curvature, in which the building up of the second molecular layer can start earlier than on a relatively flat monolayer, present at the surface of I_h ice. Finally, above the point of condensation the isotherm corresponding to amorphous ice goes again above that of I_h ice. However, in this μ range this difference simply reflects the higher density of the somewhat disordered amorphous ice than that of the I_h ice, which leaves more space for the methylamine molecules in the basic simulation box.

It should be emphasized, however, that the isotherm obtained at amorphous ice contains also the methylamine molecules that are dissolved in the ice phase, while no such dissolved molecules were found in the case of I_h ice.[47] Hence, all the observed differences of the two isotherms in all the three above discussed ranges of μ can, at least partly, be accounted for simply by the methylamine molecules dissolved in the bulk amorphous phase.

We have also converted the obtained $<N>$ vs. μ isotherms to the more conventional Γ vs. p_{rel} form, where Γ is the surface density of methylamine, calculated simply as

$$\Gamma = \frac{<N>}{2YZ},$$
(1)

and p_{rel} is the relative pressure, i.e., the ratio of the pressure of the system, p, and the pressure corresponding to the point of condensation of methylamine at the given temperature, p_0. p_{rel} can be calculated using the value of μ_0 as[34]

$$p_{rel} = \frac{p}{p_0} = \frac{\exp(\mu / k_B T)}{\exp(\mu_0 / k_B T)},$$
(2)

where k_B is the Boltzmann constant. It should be noted that since p_0 is the pressure of the saturated vapor of methylamine, isotherms can only be converted to the $\Gamma(p_{rel})$ form up to the point of condensation, i.e., when methylamine is still in its vapor phase.

The obtained isotherms are shown in the Γ vs. p_{rel} form in Figure 4 as obtained at the five temperatures considered; the corresponding values are also included in Tables S1-S5 of the supporting information. It should be emphasized again that these isotherms still contain the molecules that are dissolved in the bulk amorphous ice phase. As is seen, at a given p_{rel} value the amount of adsorbed methylamine increases with decreasing temperature, and hence at

10

lower temperatures multilayer adsorption occurs at lower p_{rel} values. It is also evident that the low pressure rising part of the isotherm becomes progressively steeper as the temperature decreases, due to the explicit dependence of p_{rel} on the temperature (see eq. 2). This steep rise of the $\Gamma(p_{rel})$ isotherm at low temperatures results in considerable surface densities of methylamine already around the relative pressure value of 10^{-30} at 20 K and 10^{-20} at 50 K. To estimate the corresponding absolute pressure range, one needs the value of p_0 at these temperatures, the value of which is clearly inaccessible from the simulations. The temperature dependence of the experimental value of p_0 is described by the Antoine equation:[75]

$$\ln p_0 = A - \frac{B}{T+C},\qquad (3)$$

(p_0 and T being in units of Pa and K, respectively), with the Antoine parameter values of $A = 21.92$, $B = 2383.1$ K, and $C = -37.574$ K, at least in the temperature range between 190 and 267 K.[76,77] On the other hand, upon going to lower temperatures, eq. 3 is expected to provide progressively worse estimate of p_0, this estimate being 1.4×10^3 Pa at 200 K, 2 Pa at 150 K, and about 10^{-7} Pa at 100 K. Using the very conservative estimate of 1 Pa for p_0 both at 20 K and 50 K, the gas phase concentration of methylamine corresponding to the above relative pressure values (i.e., 10^{-30} at 20 K and 10^{-20} at 50 K) can be estimated through $c = p/RT$ as about 10^{-35} mol/dm^3 (20 K) and 5×10^{-25} mol/dm^3 (50 K), respectively. Considering that the typical molecular number density of methylamine in the ISM is about in the order of 10^{-2} molecule/dm^3, i.e., 10^{-26} mol/dm^3,[78] our results reveal that considerable adsorption of methylamine at icy surfaces can be expected at the density and temperature characteristic of the cold part of the ISM.

The $\Gamma(p_{rel})$ isotherms obtained at 200 K at the surfaces of I$_h$ and amorphous ice are compared in the inset of Fig. 4. This comparison corroborates the conclusion drawn from the comparison of the $<N>$ vs. μ isotherms that the saturated monolayer of methylamine consists of more molecules at the surface of amorphous than at I$_h$ ice.

To better understand the nature of the adsorption, we have fitted the Langmuir isotherm:[79,80]

$$\Gamma = \Gamma_{max}\frac{p_{rel}K}{1+p_{rel}K}\qquad (4)$$

11

to the obtained Γ vs. p_{rel} data at 200 K, 150 K, and 100 K. In eq. 4, the Langmuir parameters Γ_{max} and K are the surface density of the saturated monolayer, and the Langmuir partition coefficient, measuring the affinity of the adsorbate to the surface, respectively.[79,80] The Langmuir curves fitted to the simulated data points are indicated by dashed lines in Fig. 4. As is seen, the obtained data can be reasonably well fitted up to a certain relative pressure value. This fit is never perfect, since the relatively strong lateral interaction acting between the adsorbed methylamine molecules introduces some slight deviation of the adsorption isotherms from the Langmuir form, as it was already noted in our previous study concerning I_h ice.[47] Nevertheless, the fitted curve does not deviate strongly from the data points up to the p_{rel} value of about 0.2, 0.05, and 0.02 at 200 K, 150 K, and 100 K, respectively, and this agreement also involves the beginning of the plateau part in every case. It should be emphasized, however, that, apart from the two points above $p_{rel} = 0.8$ at 200 K, all data points have always been involved in the fitting procedure, not only the ones being in the p_{rel} range of reasonably good fit. Clearly, at 200 K and 150 K the last two, while at 100 K the last three points that are used in the fitting procedure correspond to much larger Γ values than what is predicted from the fit, in spite of the fact that these points at intermediate p_{rel} values seemingly form a plateau of the isotherm. This plateau clearly could not be fitted in any case. Instead, the fitted functions, and thus also the values of the Γ_{max} parameter are determined predominantly by the low p_{rel} data points, where the assumptions underlying the Langmuir isotherm are well satisfied. This fact suggests that the difference between the plateau value of the data points and that of the fitted Langmuir isotherm reflects primarily the effect of the methylamine molecules dissolved in the bulk amorphous ice phase (and, possibly, also partly the effect of the molecules that are located at the negative local curvature troughs of the saturated first molecular layer, forming already traces of the second molecular layer). The Γ_{max} values obtained from the Langmuir fit resulted in 12.4, 12.2, and 13.0 μmol/m^2 at 200 K, 150 K, and 100 K, respectively, suggesting that the surface density of the saturated monolayer of methylamine at the surface of amorphous ice is 12.6 ± 0.4 μmol/m^2. This value is considerably higher than that corresponding to the surface of I_h ice of 10.35 μmol/m^2,[47] reflecting the fact that the corrugated surface of amorphous ice can host more adsorbed molecules in the first monolayer than the flat surface of I_h ice (This difference is also seen from the Langmuir functions fitted to the two 200 K data sets in the inset of Fig. 4.).

To check whether our above approach is correct, we have calculated the mass density profile of all methylamine molecules as well as of only those forming the first molecular layer at selected chemical potential values, using the saved sample configurations, at the five temperatures considered. The obtained profiles are shown in Figure 5. As is seen, at least at the highest chemical potential value considered at every temperature, the two profiles are markedly different from each other, indicating that at these state points the adsorption extends well beyond the first molecular layer. Assuming that the first molecular layer is already saturated in these cases, the number of molecules forming this layer can be estimated. Further, this assumption can be confirmed considering the case of condensed methylamine at 200 K (see the upper panel of Fig. 5), where this layer must be saturated. The number of methylamine molecules belonging to this saturated first molecular layer turns out to be 210 ± 20 in every case, which corresponds to the Γ value of 12.5 ± 1 $\mu mol/m^2$, being in excellent agreement with the value estimated from the Langmuir fit of 12.6 ± 0.4 $\mu mol/m^2$. The Γ values corresponding to the first molecular layer of methylamine at the selected chemical potential values, Γ^{first}, along with the corresponding p_{rel} values, are also included in Table 1.

Having the adsorbed and dissolved methylamine molecules distinguished from each other, at least at the chemical potential values at which sample configurations have been collected, the dissolution (solubility) isotherms can also be, at least, estimated. The average number of the dissolved methylamine molecules, $<N_{sol}>$, is shown as a function of the chemical potential at the five temperatures considered in Figure 6, while the inset of the figure shows these data in the c vs p_{rel} form, where c is the bulk ice phase concentration of methylamine:

$$c = \frac{<N_{sol}>}{X_{ice}YZ},$$ (5)

where the value of X_{ice}, i.e., the X range of extension of the amorphous ice phase, has been estimated to be 60 Å from the density profile of the water molecules (see Fig. 5). The c values obtained at different chemical potentials and temperatures are also included in Table 1. In interpreting the $c(p_{rel})$ solubility isotherms it should be recalled that, by performing particle insertion and deletion steps, the GCMC method efficiently removes any barrier corresponding to the direct transport of the molecules between markedly different environments (e.g., the bulk

3.2. Orientation of the First Layer Methylamine Molecules. The full description of the relative orientation of a rigid body relative to an external direction requires the use of two independent orientational variables, such as the two polar angles of the external vector in a suitably chosen coordinate frame fixed to the rigid body. Therefore, the orientational statistics of such rigid bodies, such as rigid molecules in a computer simulation, relative to an external direction can only be fully described by the bivariate joint distribution of these variables.[81,82] In analyzing the orientational preferences of the first layer methylamine molecules relative to the ice surface (or, equivalently, to the surface normal), we have chosen these variables in the following way. The frame is fixed to the individual methylamine molecules; its origin is the N atom, axis z points along the N-CH_3 bond from the N atom to the CH_3 group, axis y is parallel with the segment that joins the two hydrogen atoms of the NH_2 group, while axis x is perpendicular to the above two axes, and it is oriented in such a way that the x coordinates of the amine H atoms are positive. The orientational variables ϑ and ϕ are then the polar angles of the surface normal axis, $\underline{X}$, pointing, by our convention, away from the ice phase (see Figure 7). To analyze the orientation of the surface water molecules, we have defined the local frame, fixed to the individual water molecules, in such a way that its origin is the O atom, axis x is the molecule normal, axis y is parallel with the line connecting the two H atoms, and axis z points along the bisector of the H-O-H angle, while ϑ and ϕ are again the polar angles of $\underline{X}$ in this frame (see Fig. 7). Due to the symmetry of the methylamine and water molecules, the above frames are always chosen such that the inequalities $\phi \leq 180^{\circ}$, and $\phi \leq 90^{\circ}$, respectively are also satisfied. It should also be noted that while ϑ is the angle between two spatial vectors, ϕ is that of two planar ones (i.e., two vectors that both lay, by definition, in the xy plane of the local frame), and hence random surface orientation results in a uniform bivariate distribution only if $\cos\vartheta$ and ϕ are chosen to be the orientational variables.[81,82]

The $P(\cos\vartheta,\phi)$ orientational maps of the first layer methylamine molecules are shown in Figure 8 as obtained at selected chemical potentials at the five temperatures considered. For comparisons, orientational maps, obtained previously on I_h ice at 200 K at the same chemical potential values that are also considered here, are also shown (top row). As is seen, the obtained maps are rather noisy, especially at low temperatures and low surface coverages, due to the extremely slow exploration of the configurational space at these very low temperatures. This fact limits the range of conclusions concerning the surface orientation of the adsorbed molecules that we can reliably draw from these orientational maps. Nevertheless, it is still clear that methylamine molecules prefer orientations corresponding to the $\cos\vartheta$ value of 0, i.e., to the situation where the N-CH$_3$ bond lays parallel with the macroscopic plane of the ice surface, YZ. This preference is stronger at lower surface coverages, and smoother distributions are obtained at higher temperatures, when the larger thermal motion of the molecules results in better statistics. Among the various orientations corresponding to $\cos\vartheta = 0$, no alignment is found to be clearly preferred at every temperature and surface coverage; the maps corresponding to various state points often exhibit preferences around the ϕ values of 0º, 60º, 90º, 120º, and 180º. The alignments of the methylamine molecules corresponding to $\cos\vartheta = 0$ and these particular ϕ values are illustrated in Fig. 7. In these orientations, the methylamine molecule always turns one or two of its three hydrogen bonding directions (i.e., the two N-H bonds and the lone pair direction of the N atom) towards the ice surface. However, due to the molecular scale roughness of the surface of amorphous ice, and to the corresponding presence of pockets of locally negative curvature at the surface, the adsorbed methylamine molecules located in such pockets can easily form even three hydrogen bonds with the surface waters, especially at low surface coverages. The extensive H-bond formation between the first layer methylamine and surface water molecules is also facilitated by the fact that surface waters on amorphous ice have very weak orientational preferences, as compared to those at the surface of I_h ice, as demonstrated in Fig. 7. The orientational flexibility of the surface water molecules enables them to adopt orientations by which they can maximize the number of methylamine-water hydrogen bonds. Further, as it was discussed in detail in our previous paper,[47] the parallel alignment of the N-CH$_3$ bond with the ice surface promotes various relative alignments, corresponding to strong dipolar interaction, of the neighboring adsorbed methylamine molecules.

15

3.3. Energetics of the Adsorption. To further analyze the interaction of the adsorbed methylamine molecules both with each other and with the surface waters, and to characterize the energetic background of the adsorption, we have calculated the binding energy of the methylamine molecules belonging to the first molecular layer at the selected chemical potential values at all the five temperatures considered. The binding energy of an adsorbed molecule, U_b, is defined as its interaction energy with the rest of the system (i.e., the energy cost of bringing this molecule to infinite distance). Besides U_b, its contributions coming from the interaction with the ice phase, and with the other methylamine molecules present in the system, denoted here as U_b^{ice} and U_b^{lat}, respectively, have also been calculated.

Some of the $P(U_b)$, $P(U_b^{\text{ice}})$, and $P(U_b^{\text{lat}})$ distributions obtained at 200 K are shown and compared with the corresponding results on I_h ice[47] in Figure 9, while those obtained at 150 K, 100 K, and 50 K are shown in Figures 10.a, 10.b, and 10.c, respectively. (Similar, but considerably more noisy distributions have been obtained at 20 K.) As is expected, the lateral contribution to the total binding energy does not depend on the state of the ice phase. At low surface coverages, the main peak of the $P(U_b^{\text{lat}})$ distribution occurs at zero energy, reflecting the large fraction of isolated methylamine molecules in the adsorption layer. Besides this trivial peak, another peak can be seen around -20 kJ/mol. This peak can be attributed to neighboring methylamine dimers interacting with each other by strong dipolar interaction.[47] With increasing surface coverages, both of these peaks shift to lower energies due to the increasing background of the adsorbed methylamines, and also the relative weight of the latter, lower energy peak gradually increases. The only difference seen between the $P(U_b^{\text{lat}})$ distributions obtained on amorphous and I_h ices is that the relative weight of the lower energy peak is slightly larger in the former case. This difference can, however, simply be explained by the somewhat higher surface coverage observed on amorphous than on crystalline ice at every chemical potential (see Fig. 2).

On the other hand, the type of the ice phase has a great impact on the ice contribution of the binding energy, U_b^{ice}. At the surface of I_h ice, the $P(U_b^{\text{ice}})$ distribution exhibits a peak around -55 – -50 kJ/mol, and another one between -35 and -30 kJ/mol, attributed to the

16

methylamine molecules forming two and one hydrogen bonds with the ice phase, respectively, and with increasing surface coverage the relative weight of this latter peak increases gradually.[47] At the surface of amorphous ice, this distribution is markedly shifted to lower energies. Further, besides the above two positions, another peak of the distribution emerges between -75 and -70 kJ/mol. This peak can be attributed to methylamine molecules forming three hydrogen bonds with the ice surface. In principle, a methylamine molecule can form up to three hydrogen bonds, and could orient in such a way (i.e., turning the CH_3 group straight away from the ice surface) that all the three of its potential H-bonding directions (i.e., the two N-H bonds and the lone pair of the N atom) points towards the ice phase. However, this orientation (corresponding to the $\cos\vartheta = 1$ line of the orientational maps of Fig. 8) was found not to be preferred at all both on crystalline,[47] and on amorphous ice. The reason of the lack of preference for this orientation is probably that it hinders the formation of strong dipolar pairs by the neighboring adsorbed methylamine molecules (or, more precisely, the formation of such a dipolar pair in the first molecular layer would imply very weak interaction of the other methylamine molecule with the ice phase).[47] On the other hand, the molecular level corrugation of the surface of amorphous ice offers certain positions of locally negative curvature (i.e., molecular size troughs), within which the adsorbed methylamine molecule can still maintain all of its three possible hydrogen bonds. It is also seen from Fig. 9 that the increase of the surface density leads both to the slight shift of the position of the $P(U_b^{ice})$ peaks to higher energies, and to the increase of the relative weights of the peaks corresponding to smaller number of hydrogen bonds. Both effects can be explained by the increasing competition of the methylamine molecules at the surface.

The heat of the adsorption at infinitely low surface coverage, an experimentally accessible quantity, can be estimated by the mean value of the $P(U_b^{ice})$ distribution at low enough surface coverages, where the lateral interaction is small enough with respect to the adsorbate-adsorbent interaction. Using the lowest sampled chemical potential in every case, this value turns out to be -72 kJ/mol at 200 K, and scatters between -65 and -75 kJ/mol at the other temperatures considered, showing no apparent temperature dependence; its temperature independent value is estimated here to be -69 ± 5 kJ/mol. By contrast, at the surface of I_h ice this value was found to be only -51.3 kJ/mol,[47] emphasizing again the higher affinity of methylamine to the surface of amorphous than to that of crystalline ice. Unfortunately, we are

not aware of any experiment in which this value is accessed at infinitely low surface coverage. The binding energy of methylamine on amorphous ice was, however, estimated in the very recent paper of Chaabouni et al.[83] at higher surface coverages. In a clear accordance with our results, they obtained a trimodal distribution at the surface coverage corresponding to 32% of the saturated monolayer, with the mean values of the peaks corresponding roughly to -35, -45, and -61 kJ/mol (see Fig. 7 of Ref. 83). Similar, although somewhat lower values are obtained here when considering chemical potential values corresponding to similar surface coverages (e.g., -34, -52, and -71 kJ/mol at 100 K). At the lowest surface coverage considered, corresponding to 15% of the saturated monolayer, Chaabouni et al. estimated the binding energy to be -50 kJ/mol,[83] which is considerably smaller in magnitude than our estimate of -69 ± 5 kJ/mol. However, our value is derived from configurations corresponding to the surface coverage values of 0.18-0.36 μmol/m^2, which, considering our estimate of 12.6 μmol/m^2 for the saturated monolayer (see sec. 3.1), corresponds to only 1.5-3% of the saturated monolayer. This one order of magnitude difference between the surface coverages can largely explain the above difference between our result and the value reported by Chaabouni et al. It should also be noted that Chaabouni et al. measured the surface desorption rate of methylamine, and derived the binding energy distribution using several model assumptions.[83] Nevertheless, this comparison also leaves open the possibility that the potential model combination used in the present study somewhat overestimates the adhesion between the ice surface and the methylamine molecules. It should also be noted that the experimental value of the activation energy of the methylamine desorption reported by Chaabouni et al. as well as the heat of adsorption value estimated from our simulations, considering either amorphous or crystalline ice, are a factor of 2-3 larger than the speculative value of -25 kJ/mol, estimated by Vinogradoff *et al.*, assuming that the desorption activation energy of methylamine is identical to that of ammonia.[21]

Due to the larger ice contribution, the total binding energy distribution, $P(U_b)$, is also shifted to lower energies when going from crystalline to amorphous ice. Interestingly, the distributions obtained at various surface coverages are rather similar to each other, indicating that the weakening of the adsorbate-ice interaction is fully compensated by the increase of the lateral interaction upon increasing the surface coverage. At lower temperatures, the obtained

$P(U_b)$ curves exhibit two distinguishable peaks, still reflecting the presence of methylamine molecules forming two and three hydrogen bonds with the surface waters.

The binding energy distributions obtained at lower temperatures show the same general picture, with no apparent temperature dependence of their features. The only clear effect of the temperature decrease is that the distributions become more structured, and their peaks get sharper. Although this effect can be explained by the decreasing weight of the entropy term of the free energy of the system, it is presumably also, at least partly, due to the worsening of the sampling due to the decreased mobility of the molecules at lower temperatures.

Besides that of the adsorption layer, we have also investigated the energetics of the methylamine molecules that are dissolved in the bulk ice phase. The bulk phase concentration of these molecules is always small enough that the lateral contribution to their binding energy is nearly zero. Therefore, here we only discuss the distribution of the ice contribution, U_b^{ice}. The $P(U_b^{ice})$ distribution of the dissolved molecules is shown in Figure 11 in all cases when it is not affected by too large statistical noise. The distributions do not show apparent dependence on the chemical potential (as the corresponding bulk ice concentration is always small enough); the observed differences can rather be attributed to the poor sampling due to the small number of the dissolved molecules.

At 200 K, the obtained $P(U_b^{ice})$ distributions are smooth and unimodal, having their peak between -80 and -85 kJ/mol. At lower temperatures, peaks corresponding to methylamines forming two and three hydrogen bonds with the surrounding water molecules can, in some cases, be distinguished. The overall picture is rather similar to what has been seen in the first adsorbed monolayer, with a shift of the entire distributions to about -10 kJ/mol lower energies. The energy of solvation at infinite dilution, obtained considering the $P(U_b^{ice})$ distribution in all cases when the $P(U_b^{lat})$ distribution (not shown) does not extend below -5 kJ/mol, has turned out to be -74 ± 7 kJ/mol. This value is only about 5 kJ/mol deeper than what is obtained in the surface monolayer, emphasizing again that at low enough surface coverages methylamine molecules can be accommodated in pockets of locally negative curvature of the surface, in which their local environment can be rather similar to that inside the bulk ice phase.

4. Summary and Conclusions

In this paper, we presented a detailed computer simulation analysis of the adsorption of methylamine at the surface of amorphous ice at low temperatures, some of which are relevant in studying processes occurring in the ISM. Our results clearly showed that methylamine has a strong ability of being adsorbed at such surfaces, which leads even to multilayer adsorption at high enough relative pressures. The adsorption was found to be strongly enhanced by the decrease of the temperature, thus, in the temperature range of 20-50 K, characteristic of a large part of the space, considerable surface densities can be reached even at as low bulk gas phase concentrations that occur in the ISM. It should be emphasized, however, that our simulations access only the state of thermodynamic equilibrium, but can say nothing about the kinetics of the adsorption. In other words, we found that at the low temperatures and concentrations characteristic to the ISM icy surfaces may well contain a considerable amount of adsorbed methylamine in equilibrium, but have no access to the time scale within which this equilibrium can be reached under the extreme conditions of the ISM.

When comparing our present results with those obtained earlier at the surface of crystalline (I_h) ice under similar conditions,[47] we found a considerably higher adsorption capacity of the amorphous ice surface than that of I_h ice, primarily due to the larger surface area of the amorphous phase, resulted from the corrugation of its surface. This increase of the surface area is estimated to be as large as 20% from the surface densities of the saturated monolayer, being 10.35 μmol/m^2 on crystalline,[47] while about 12.5 μmol/m^2 on amorphous ice. Further, besides its increased adsorption capacity, it is also found that amorphous ice, unlike I_h ice,[47] is able to dissolve a noticeable amount of methylamine. This finding is in a clear accordance with the experimental finding of Vinogradoff et al.[21]

When analyzing the orientation and energetics of the methylamine molecules forming the first molecular layer, we found that the aforementioned enhanced adsorption capacity of amorphous ice is coupled with its ability of binding methylamine molecules considerably stronger than I_h ice. Thus, due to the molecular size roughness of the surface of amorphous ice (i.e., the presence of troughs), and to the almost negligible orientational preference of the surface water molecules, the first layer methylamine molecules can easily form even three hydrogen bonds with the surface water molecules, at least at low enough surface coverages.

20

This behavior is in a clear contrast with our earlier finding on I_h ice, where the adsorbed molecules do not form more than two such H-bonds. This difference is also reflected in the estimated heat of adsorption values at infinitely low surface coverage of -51.3 kJ/mol (on I_h ice)[47] and -69 ± 5 kJ/mol (on amorphous ice). This latter value is rather close to the estimated heat of solvation of -74 ± 7 kJ/mol in the bulk amorphous ice phase, confirming again that at the rough surface of amorphous ice, consisting of water molecules with no particular pre-defined orientational preferences, methylamine molecules at low surface coverages experience an almost bulk-like local environment. Finally, it has to be pointed out that the heat of adsorption, estimated at the surface of both I_h and amorphous ice, is considerably lower than the speculative value of Vinogradoff et al. of -25 kJ/mol,[21] revealing that the crude assumption of considering this value to be identical with that of NH_3, made in this latter study,[21] clearly represents a serious oversimplification of the real situation.

Supporting Information. Numerical data of the calculated adsorption isotherms. This material is available free of charge via the Internet at http://pubs.acs.org.

References

(1) Oro, J. Comets and the Formation of Biochemical Compounds on the Primitive Earth. *Nature* **1961,** *190*, 389-390.

(2) Brack, A. Life in the Solar System. *Adv. Space Res.* **1999,** *24,* 417-433.

(3) Meierhenrich, U.; Thiemann, W. H. P.; Rosenbauer, H. Molecular Parity Violation via Comets? *Chirality* **1999,** *11,* 575–582.

(4) Newton, D. E. *Chemistry of Space in Series New Chemistry;* Facts on File Inc.: New York, 2007.

(5) Kim, Y. S.; Kaiser, R. I. On the Formation of Amines (RNH_2) and the Cyanide Anion (CN^-) in Electron-Irradiated Ammonia–Hydrocarbon Interstellar Model Ices. *Astrophys. J.* **2011,** *729*, 68.

(6) Förstel, M.; Bergantini, A.; Maksyutenko, P.; Góbi, S.; Kaiser, R. I. Formation of Methylamine and Ethylamine in Extraterrestrial Ices and Their Role as Fundamental Building Blocks of Proteinogenic α-Amino Acids. *Astrophys. J.* **2017,** *845*, 83.

(7) Theule, P.; Borget, F.; Mispelaer, F.; Danger, G.; Duvernay, F.; Guillemin, J. C.; Chiavassa, T. Hydrogenation of Solid Hydrogen Cyanide HCN and Methanimine CH_2NH at Low Temperature. *Astron. Astrophys.* **2011,** *534*, A64.

(8) Woon, D. E. Pathways to Glycine and Other Amino Acids in Ultraviolet-Irradiated Astrophysical Ices Determined via Quantum Chemical Modeling. *Astrophys. J. Letters* **2002,** *571*, L177-L180.

(9) Holtom, P. D.; Bennett, C. J.; Osamura, Y.; Mason, N. J.; Kaiser, R. I. A Combined Experimental and Theoretical Study on the Formation of the Amino Acid Glycine (NH_2CH_2COOH) and Its Isomer ($CH_3NHCOOH$) in Extraterrestrial Ices. *Astrophys. J.* **2005,** *626*, 940-952.

(10) Kaiser, R. I.; Stockton, A. M.; Kim, Y. S.; Jensen, E. C.; Mathies, R. A. On the Formation of Dipeptides in Interstellar Model Ices. *Astrophys. J.* **2013,** *765*, 111.

(11) Glavin, D. P.; Dworkin, J. P.; Sandford, S. A. Detection of Cometary Amines in Samples Returned by Stardust *Meteorit. Planet. Sci.* **2008,** *43,* 399-413.

(12) Goesmann, F.; Rosenbauer, H.; Bredehöft, J. H.; Cabane, M.; Ehrenfreund, P.; Gautier, T.; Giri, C.; Krüger, H.; Le Roy, L.; MacDermott, A. J.; McKenna-Lawlor, S.; Meierhenrich, U. J.; Muñoz-Caro, G. M.; Raulin, F.; Roll, R.; Steele, A.; Steininger, H.;

Sternberg, R.; Szopa, C.; Thiemann, W.; Ulamec, S. Organic Compounds on Comet 67P/Churyumov-Gerasimenko Revealed by COSAC Mass Spectrometry. *Science* **2015,** *349*, aab0689.

(13)   Aponte, J. C.; Elsila, J. E.; Glavin, D. P.; Milam, S. N.; Charnley, S. B.; Dworkin, J. P., Pathways to Meteoritic Glycine and Methylamine. *ACS Earth Space Chem.* **2017,** *1*, 3-13.

(14)   Jungclaus, G. A.; Cronin, J. R.; Moore, C. B.; Yuen, G. U. Aliphatic Amines in the Murchison Meteorite. *Nature* **1976,** *261*, 126-128.

(15)   Pizzarello, S.; Feng, X.; Epstein, S.; Cronin, J. R. Isotopic Analyses of Nitrogenous Compounds from the Murchison Meteorite: Ammonia, Amines, Amino Aacids, and Polar Hydrocarbons. *Geochim. Cosmochim. Acta* **1994,** *58*, 5579-5587.

(16)   Pizzarello, S.; Holmes, W. Nitrogen-Containing Compounds in two CR2 Meteorites: 15N Composition, Molecular Distribution and Precursor Molecules. *Geochim. Cosmochim. Acta* **2009,** *73*, 2150−2162.

(17)   Aponte, J. C.; Dworkin, J. P.; Elsila, J. E. Indigenous Aliphatic Amines in the Aqueously Altered Orgueil Meteorite. *Meteorit. Planet. Sci.* **2015,** *50*, 1733–1749.

(18)   Cottin, H.; Gazeau, M. C.; Raulin, F. Cometary Organic Chemistry: A Review from Observations Numerical and Experimental Simulations. *Planet. Space Sci.* **1999,** *47*, 1141–1162.

(19)   Mispelaer, F.; Theule, P.; Aouididi, H.; Noble, J.; Duvernay, F.; Danger, G.; Roubin, P.; Morata, O.; Hasegawa, T.; Chiavassa, T.; Diffusion Measurements of CO, HNCO, H_2CO, and NH_3 in Amorphous Water Ice. *Astron. Astrophys.* **2013,** *555*, A13.

(20)   Danger, G.; Rimola, A.; Abou Mrad, N; Duvernay, F.; Roussin, G; Theule, P.; Chiavassa, T. Formation of Hydroxyacetonitrile ($HOCH_2CN$) and Polyoxymethylene (POM)-Derivatives in Comets from Formaldehyde (CH_2O) and Hydrogen Cyanide (HCN) Activated by Water. *Phys. Chem. Chem. Phys.* **2014,** *16*, 3360-3370.

(21)   Vinogradoff, V.; Duvernay, F.; Danger, G.; Theulé, P.; Borget, F.; Chiavassa T. Formaldehyde and Methylamine Reactivity in Interstellar Ice Analogues As a Source of Molecular Complexity At Low Temperature. *Astron. Astrophys.* **2013,** 549, A40.

(22)   Cuppen, H. M.; Walsh, C.; Lamberts, T.; Semenov, D.; Garrod, R. T.; Penteado, E. M.; Ioppolo, S. Grain Surface Models and Data for Astrochemistry. *Space Sci. Rev.* **2017,** *212*, 1–58.

(23)   Allen, M. P.; Tildesley, D. J. *Computer Simulation of Liquids*; Clarendon: Oxford, 1987.

(24)   Adams, D. J. Grand Canonical Ensemble Monte Carlo for a Lennard-Jones Fluid. *Mol. Phys.* **1975,** *29,* 307-311.

(25)   Samios, S.; Stubos, A. K.; Kanellopoulos, N. K.; Cracknell, R. F.; Papadopoulos, G. K.; Nicholson, D. Determination of Micropore Size Distribution from Grand Canonical Monte Carlo Simulations and Experimental CO_2 Isotherm Data. *Langmuir* **1997,** *13,* 2795-2802.

(26)   Muller, E. A.; Hung, F. R.; Gubbins, K. E. Adsorption of Water Vapor-Methane Mixtures on Activated Carbons. *Langmuir* **2000,** *16,* 5418-5424.

(27)   Challa, S. R.; Sholl, D. S.; Johnson, J. K. Adsorption and Separation of Hydrogen Isotopes in Carbon Nanotubes: Multicomponent Grand Canonical Monte Carlo Simulations. *J. Chem. Phys.* **2002,** *116,* 814-824.

(28)   Striolo, A.; Chialvo, A. A.; Gubbins, K. E.; Cummings, P. T. Water in Carbon Nanotubes: Adsorption Isotherms and Thermodynamic Properties from Molecular Simulation. *J. Chem. Phys.* **2005,** *122,* 234712.

(29)   Moulin, F.; Picaud, S.; Hoang, P. N. M.; Jedlovszky, P. Grand Canonical Monte Carlo Simulation of the Adsorption Isotherms of Water Molecules on a Model Soot Particle *J. Chem. Phys.* **2007,** *127,* 164719.

(30)   Hantal, Gy.; Picaud, S.; Hoang, P. N. M.; Voloshin, V. P.; Medvedev, N. N.; Jedlovszky, P. Water Adsorption Isotherms on Porous Onionlike Carbonaceous Particles. Simulations with the Grand Canonical Monte Carlo Method. *J. Chem. Phys.* **2010,** *133,* 144702.

(31)   Firlej, L.; Kuchta, B.; Lazarewicz, A.; Pfeifer, P. Increased H_2 Gravimetric Storage Capacity in Truncated Carbon Slit Pores Modeled by Grand Canonical Monte Carlo. *Carbon* **2013,** *53*, 208-215.

(32)   Puibasset, J.; Pellenq, R. J. M. Water Adsorption on Hydrophilic Mesoporous and Place Silica Substrates: a Grand Canonical Monte Carlo Simulation Study. *J. Chem. Phys.* **2003,** *118,* 5613-5622.

(33) Puibasset, J.; Pellenq, R. J. M. Water Adsorption in Disordered Mesoporous Silica (Vycor) at 300 K and 650 K : A Grand Canonical Monte Carlo Simulation Study of Hysteresis. *J. Chem. Phys.* **2005,** *122,* 094704.

(34) Daub, C. D.; Patey G. N.; Jack, D. B.; Sallabi A. K. Monte Carlo Simulations of the Adsorption of CO_2 on the MgO(100) Surface. *J. Chem. Phys.* **2006,** *124,* 114706.

(35) Tombácz, E.; Hajdú, A.; Illés, E.; László, K.; Garberoglio, G.; Jedlovszky, P. Water in Contact with Magnetite Nanoparticles, as Seen from Experiments and Computer Simulations. *Langmuir* **2009,** *25,* 13007-13014.

(36) Jung, D. H.; Kim, D.; Lee, T. B.; Choi, S. B.; Yoon, J. H.; Kim, J.; Choi, K.; Choi, S. H. Grand Canonical Monte Carlo Simulation Study on the Catenation Effect on Hydrogen Adsorption onto the Interpenetrating Metal-Organic Frameworks. *J. Phys. Chem. B* **2006,** *110*, 22987-22990.

(37) Garberoglio, G. Computer Simulation of the Adsorption of Light Gases in Covalent Organic Frameworks. *Langmuir* **2007,** *23,* 12154-12158.

(38) Ramsahye, N. A.; Maurin, G.; Bourelly, S.; Llewellyn, P. L.; Devic, T.; Serre, C.; Loiseau, T.; Ferey, G. Adsorption of CO_2 in Metal Organic Frameworks of Different Metal Centres: Grand Canonical Monte Carlo Simulations Compared to Experiments. *Adsorption* **2007,** *13*, 461-467.

(39) Jedlovszky, P.; Partay, L.; Hoang, P. N. M.; Picaud, S.; von Hessberg, P.; Crowley, J. N. Determination of the Adsorption Isotherm of Methanol on the Surface of Ice. An Experimental and Grand Canonical Monte Carlo Simulation Study. *J. Am. Chem. Soc.* **2006**, *128*, 15300-15309.

(40) Hantal, G.; Jedlovszky, P.; Hoang, P.N.M.; Picaud, S. Investigation of the Adsorption Behavior of Acetone at the Surface of Ice. A Grand Canonical Monte Carlo Simulation Study. *Phys. Chem. Chem. Phys.* ***2008,** 10,* 6369-6380.

(41) Jedlovszky, P.; Hantal, Gy.; Neuróhr, K.; Picaud, S.; Hoang, P. N. M.; von Hessberg, P.; Crowley, J. N. Adsorption Isotherm of Formic Acid on The Surface of Ice, as Seen from Experiments and Grand Canonical Monte Carlo Simulation. *J. Phys. Chem. C* **2008,** *112*, 8976-8987.

(42)   Petitjean, M.; Hantal, Gy.; Chauvin, C.; Mirabel, P.; Le Calvé, S.; Hoang, P. N. M.; Picaud, S.; Jedlovszky, P. Adsorption of Benzaldehyde at the Surface of Ice, Studied by Experimental Method and Computer Simulation. *Langmuir* **2010,** *26,* 9596-9606.

(43)   Mészár, Zs. E.; Hantal, Gy.; Picaud, S.; Jedlovszky, P. Adsorption of Aromatic Hydrocarbon Molecules at the Surface of Ice, As Seen by Grand Canonical Monte Carlo Simulation. *J. Phys. Chem. C* **2013,** *117*, 6719-6729.

(44)   Szőri, M.; Jedlovszky, P. Adsorption of HCN at the Surface of Ice. A Grand Canonical Monte Carlo Simulation Study. *J. Phys. Chem. C* **2014,** *118*, 3599-3609.

(45)   Sumi, I.; Picaud, S.; Jedlovszky, P. Adsorption of Methylene Fluoride and Methylene Chloride at the Surface of Ice under Tropospheric Conditions. A Grand Canonical Monte Carlo Simulation Study. *J. Phys. Chem. C* **2015,** *119*, 17243-17252.

(46)   Sumi, I.; Fábián, B.; Picaud, S.; Jedlovszky, P. Adsorption of Fluorinated Methane Derivatives at the Surface of Ice under Tropospheric Conditions, As Seen from Grand Canonical Monte Carlo Simulations. *J. Phys. Chem. C* **2016,** *120*, 17386-17399.

(47)   Szentirmai, V.; Szőri, M.; Picaud, S.; Jedlovszky, P. Adsorption of Methylamine at the Surface of Ice. A Grand Canonical Monte Carlo Simulation Study *J. Phys. Chem. C* **2016,** *120*, 23480-23489.

(48)   Sumi, I.; Picaud, S.; Jedlovszky, P. Adsorption of Chlorinated Methane Derivatives at the Ice Surface: A Grand Canonical Monte Carlo Simulation Study. *J. Phys. Chem. C* **2017,** *121*, 7782-7793.

(49)   Fábián, B.; Picaud, S.; Jedlovszky, P.; Guilbert-Lepoutre, A.; Moussis, O. Ammonia Clathrate Hydrate As Seen from Grand Canonical Monte Carlo Simulations. *ACS Earth and Space Chemistry*, in press.

(50)   Rutkai, G.; Kristóf, T. Molecular Simulation Study of Intercalation of Small Molecules in Kaolinite. *Chem. Phys. Letters* **2008**, *462*, 269-274.

(51)   Croteau, T.; Bertram, A. K.; Patey, G. N. Adsorption and Structure of Water on Kaolinite Surfaces: Possible Insight into Ice Nucleation from Grand Canonical Monte Carlo Calculations. *J. Phys. Chem. A* **2008,** *112,* 10708-10712.

(52)   Jameson, C. J.; Jameson, K.; Baello, B. I.; Lim, H. M. Grand Canonical Monte Carlo Simulations of the Distribution and Chemical Shifts of Xenon in the Cages of Zeolite NaA. 1. Distribution and Xe-129 Chemical Shifts. *J. Chem. Phys.* **1994,** *100,* 5965-5976.

(53)   Jameson, C. J.; Jameson, K.; Lim, H. M.; Baello, B. I. Grand Canonical Monte Carlo Simulations of the Distribution and Chemical Shifts of Xenon in the Cages of Zeolite NaA. 2. Structure of the Adsorbed Fluid. *J. Chem. Phys.* **1994**, *100,* 5977-5987.

(54)   Smit, B. Grand Canonical Monte Carlo Simulations of Chain Molecules: Adsorption Isotherms of Alkanes in Zeolites. *Mol. Phys.* **1995,** *85*, 153-172.

(55)   Pellenq, R. J. M.; Tavitian, B.; Espinat, D.; Fuchs, A. H. Grand Canonical Monte Carlo Simulations of Adsorption of Polar and Nonpolar Molecules in NaY Zeolite. *Langmuir* **1996,** *12,* 4768-4783.

(56)   Macedonia, M. D.; Maginn, E. J. Pure and Binary Component Sorption Equilibria of Light Hydrocarbons in the Zeolite Silicalite from Grand Canonical Monte Carlo Simulations. *Fluid Phase Equil.* **1999,** *158-160*, 19-27.

(57)   Rutkai, G.; Csányi, É.; Kristóf, T. Prediction of Adsorption Equilibria of Water-Methanol Mixtures in Zeolite NaA by Molecular Simulation. *Mol. Simul.* **2006,** *32*, 869-875.

(58)   Kristóf, T.; Csányi, É.; Rutkai, G. Prediction of Adsorption and Separation of Water-Alcohol Mixtures with Zeolite NaA. *Microporous Mesoporous Mat.* **2008,** *114*, 455-464.

(59)   Szőri, M.; Jedlovszky, P.; Roeselová, M. Water Adsorption on Hydrophilic and Hydrophobic Self-Assembled Monolayers as Proxies For Atmospheric Surfaces. A Grand Canonical Monte Carlo Simulation Study. *Phys. Chem. Chem. Phys.* **2010,** *12*, 4604-4616.

(60)   Szőri, M.; Roeselová, M.; Jedlovszky, P. Surface Hydrophilicity-Dependent Water Adsorption on Mixed Self-Assembled Monolayers of C_7-CH_3 and C_7-COOH residues. A Grand Canonical Monte Carlo Simulation Study. *J. Phys. Chem. C* **2011,** *115*, 19165-19177.

(61)   Resat, H.; Mezei, M. Grand Canonical Monte Carlo Simulation of Water Positions in Crystal Hydrates. *J. Am. Chem. Soc.* **1994**, *116*, 7451-7452.

(62)   Ge, X.; Wexler, A. S.; Clegg, S.L. Atmospheric Amines – Part I. A Review. *Atmos. Environ.* **2011**, *45*, 524-546.

(63)   Solomon, S.; Garcia, R. R.; Rowland, F. S.; Wuebbles, D. J. On the Depletion of Antarctic Ozone. *Nature* **1986**, *321*, 755-758.

(64) Yu, F.; Luo. G. Modeling of Gaseous Methylamines in the Global Atmosphere: Impacts of Oxidation and Aerosol Uptake. *Atmos. Chem. Phys.* **2014**, *14*, 12455-12464.

(65) Mahoney, M.; Jorgensen, W. L. A Five-Site Model for Liquid Water and the Reproduction of the Density Anomaly by Rigid, Nonpolarizable Potential Functions. *J. Chem. Phys.* **2000,** *112*, 8910-8922.

(66) Impey, R. W.; Sprik, M.; Klein, M. L. Ionic Solvation in Nonaqueous Solvents: The Structure of Li^+ and Cl^- in Methanol, Ammonia, and Methylamine. *J. Am. Chem. Soc.* **1987,** *10*9, 5900-5904.

(67) Vega, C.; Abascal, J. L. F.; Conde, M. M.; Aragones, J. L. What Ice Can Teach Us about Water Interactions: A Critical Comparison of the Performance of Different Water Models. *Faraday Discuss.* **2009,** *141*, 251-276.

(68) Brovchenko, I.; Geiger, A.; Oleinikova, A Liquid-Liquid Phase Transition in Supercooled Water Studied by Computer Simulations of Various Water Models. *J. Chem. Phys.* **2005,** *123*, 044515.

(69) Mezei, M. *MMC: Monte Carlo Program for Simulation of Molecular Assemblies.* URL: http://inka.mssm.edu/~mezei/mmc.

(70) Mezei, M. A Cavity-Biased (T, V, μ) Monte Carlo Method for the Computer-Simulation of Fluids. *Mol. Phys.* **1980,** *40,* 901-906.

(71) Mezei, M. Grand Canonical Ensemble Monte Carlo Study of Dense Liquid Lennard-Jones, Soft Spheres and Water. *Mol. Phys.* **1987,** *61,* 565-582. Erratum: **1989,** *67,* 1207-1208.

(72) Metropolis, N.; Rosenbluth, A. W.; Rosenbluth, M. N.; Teller, A. H.; Teller, E. Equation of State Calculations by Fast Computing Machines *J. Chem. Phys.* **1953,** *21* 1087-1093.

(73) Jorge, M.; Jedlovszky, P.; Cordeiro, M. N. D. S. A Critical Assessment of Methods for the Intrinsic Analysis of Liquid Interfaces. 1. Surface Site Distributions. *J. Phys. Chem. C.* **2010,** *114*, 11169-11179.

(74) Pártay, L. B.; Hantal, Gy.; Jedlovszky, P.; Vincze, Á.; Horvai, G. A New Method for Determining the Interfacial Molecules and Characterizing the Surface Roughness in Computer Simulations. Application to the Liquid–Vapor Interface of Water. *J. Comp. Chem.* **2008,** *29,* 945-956.

(75)   Thomson, G. W. The Antoine Equation for Vapor-Pressure Data. *Chem. Rev.* **1946,** *38*, 1-39.

(76)   Aston, J. G.; Siller, C. W.; Messerly, G. H. Heat Capacities and Entropies of Organic Compounds. III. Methylamine from 12 K to the Boiling Point. Heat of Vaporization and Vapor Pressure. The Entropy from Molecular Data. *J. Am. Chem. Soc.* **1937,** *59*, 1743-1751.

(77)   *NIST Chemistry WebBook, SRD 69.* URL: http://webbook.nist.gov/cgi/cbook.cgi?ID=C74895&Mask=4&Type=ANTOINE&Plot=on

(78)   Halfen, D. T.; Ilyushin, V. V.; Ziurys, L. M. Insight into Surface Hydrogenation in the Interstellar Medium: Observations of Methanimine and Methyl Amine in Sgr B2(N). *Astrophys. J.* **2013,** *767*, 66.

(79)   Langmuir, I. The Constitution and Fundamental Properties of Solids and Liquids. Part I: Solids. *J. Am. Chem. Soc.* **1916,** *38*, 2221-2295.

(80)   Shaw, D. J. *Introduction to Colloid and Surface Chemistry*, Butterworths: London, 1980.

(81)   Jedlovszky, P.; Vincze, Á.; Horvai, G. New Insight into the Orientational Order of Water Molecules at the Water/1,2-Dichloroethane Interface: A Monte Carlo Simulation Study. *J. Chem. Phys.* **2002,** *117,* 2271-2280.

(82)   Jedlovszky, P.; Vincze, Á.; Horvai, G. Full Description of the Orientational Statistics of Molecules Near to Interfaces. Water at the Interface with CCl_4. *Phys. Chem. Chem. Phys.* **2004,** *6,* 1874-1879.

(83)   Chaabouni, H.; Diana, S.; Nguyen, T.; Dulieu, F. Thermal Desorption of Formamide and Methylamine from Graphite and Amorphous Water Ice Surfaces. *Astron. Astrophys.*, in press.

Tables

Table 1. Properties of the System at the Thermodynamic State Points Where Sample Configurations Have Been Collected for Detailed Analyses.

T/K	μ/kJ mol^{-1}	$<N>$	p_{rel}	I^{first}/μmol m^{-2}	c/mol dm^{-3}
	-47.87	6.010	3.48×10^{-57}	0.445	0
20	-39.56	48.55	1.80×10^{-35}	2.94	3.96×10^{-2}
	-32.08	145.4	6.31×10^{-16}	8.58	7.94×10^{-2}
	-28.75	265.8	3.06×10^{-7}	11.2	0.1272
	-50.83	5.263	7.88×10^{-25}	0.391	0
50	-42.10	44.21	1.04×10^{-15}	3.00	1.98×10^{-2}
	-34.62	143.1	6.83×10^{-8}	9.55	0.1091
	-29.63	305.1	1.11×10^{-2}	11.5	0.1189
	-49.32	5.964	1.03×10^{-10}	0.395	3.57×10^{-2}
100	-43.50	49.77	1.13×10^{-7}	3.41	3.96×10^{-2}
	-37.68	151.4	1.23×10^{-4}	9.26	0.1208
	-31.86	305.4	0.135	11.7	0.1525
	-51.05	4.942	3.06×10^{-7}	0.354	5.55×10^{-5}
150	-43.57	46.56	1.23×10^{-4}	3.20	2.58×10^{-2}
	-39.83	124.8	2.48×10^{-3}	7.46	0.1189
	-33.59	237.7	0.368	11.4	0.3514
	-50.49	3.089	3.91×10^{-5}	0.159	1.48×10^{-2}
	-47.17	18.50	2.89×10^{-4}	1.01	6.68×10^{-2}
	-42.18	96.12	5.80×10^{-3}	5.20	0.2496
200	-38.85	169.7	4.29×10^{-2}	8.67	0.5348
	-35.53	238.1	0.317	12.1	0.7131
	-33.78	330.5	0.905	13.9	1.064
	-33.03	921.1		12.9	0.7528

Figure Legend

Figure 1. Equilibrium snapshots of the system simulated at 20 K, as obtained at four selected chemical potential values, shown both from top and side views. Water O atoms are represented by red balls, while methylamine molecules dissolved in the ice phase, being in the first monolayer at the ice surface, and being in outer molecular layers of the adsorbed phase are shown by dark blue, yellow, and cyan colors, respectively.

Figure 2. Adsorption isotherms of methylamine on amorphous ice, shown in the form of average number of molecules in the basic box as a function of the chemical potential, as obtained from our sets of GCMC simulations at the five temperatures considered. Circles, black color: $T = 200$ K, squares, red color: $T = 150$ K, up triangles, green color: $T = 100$ K, down triangles, blue color: $T = 50$ K, diamonds, orange color: $T = 20$ K. The lines connecting the points are just guides to the eye. The state points at which sample configurations have been collected for detailed analyses are marked by arrows; the corresponding chemical potential values are also indicated. The inset compares the isotherm obtained here at 200 K (filled circles) with that obtained previously at this temperature on crystalline I_h ice (Ref. 47, open circles). All data points include also the molecules that are dissolved in the bulk ice phase.

Figure 3. The chemical potential of methylamine corresponding to the point of condensation as a function of the temperature, as obtained from our GCMC simulations (filled circles). The straight line fitted to these points is also shown (dashed line).

Figure 4. Adsorption isotherms of methylamine on amorphous ice, shown in the form of surface density vs. relative pressure, as obtained from our sets of GCMC simulations at the five temperatures considered. Black circles: $T = 200$ K, red squares: $T = 150$ K, green up triangles: $T = 100$ K, blue down triangles: $T = 50$ K, orange diamonds: $T = 20$ K. The lines connecting the points are just guides to the eye. The Langmuir isotherms fitted to the 200 K, 150 K, and 100 K data are shown by dashed lines of the respective colors. The inset compares the isotherm obtained here at 200 K (filled circles) with that obtained previously at this temperature on crystalline I_h ice (Ref. 47, open circles), together with the Langmuir isotherms fitted to them. All data points include also the molecules that are dissolved in the bulk ice phase.

Figure 5. Mass density profiles of all methylamine molecules present in the basic box (solid curves) and of those forming the first monolayer at the ice surface (full circles) along the interface normal axis, *X,* obtained at selected chemical potential values at 200 K (top panel), 150 K (second panel), 100 K (third panel), 50 K (fourth panel), and 20 K (bottom panel). For reference, the density profile of the water molecules forming the ice phase is also shown (thick dashed line). All profiles shown are symmetrized over the two interfaces present in the basic box.

Figure 6. Dissolution isotherms of methylamine in amorphous ice, shown in the form of average number of dissolved molecules in the basic box as a function of the chemical potential, as obtained from our sets of GCMC simulations at the five temperatures considered. Black circles: $T = 200$ K, red squares: $T = 150$ K, green up triangles: $T = 100$ K, blue down triangles: $T = 50$ K, orange diamonds: $T = 20$ K. The lines connecting the points are just guides to the eye. The inset shows the same isotherms, in the form of bulk concentration vs. relative pressure.

Figure 7. Definition of the local frame fixed to the individual methylamine (top left) and water (top right) molecules, and of the polar angles ϑ and ϕ of the surface normal vector pointing, by our convention, away from the ice phase, $\underline{X}$, in these frames (see the text). Illustration of the preferred alignments of the surface methylamine molecules relative to the surface normal vector, $\underline{X}$ (bottom left). Orientational maps of the water molecules at the surface of crystalline (I_h) ice and amorphous ice, together with the illustration of the orientations preferred at I_h ice (bottom right). In the orientational maps, lighter colors correspond to higher probabilities.

Figure 8. Orientational maps of the first layer methylamine molecules at the surface of crystalline (I_h) ice at 200 K (top row, Ref. 47) as well as at the surface of amorphous ice at 200 K (second row), 150 K (third row), 100 K (fourth row), 50 K (fifth row), and 20 K (bottom row), as obtained at selected chemical potential values. In the maps, lighter colors correspond to higher probabilities.

Figure 9. Distribution of the total binding energy of the first layer methylamine molecules (bottom panel), as well as its contributions coming from the interaction with the other methylamine molecules in the system (middle panel) and with the ice phase (top panel), as obtained at 200 K at the surface of crystalline (I_h) ice (open symbols, Ref. 47), and at that of amorphous ice (full symbols) at the chemical potential values of -35.5 kJ/mol (red), -42.2 kJ/mol (blue), and -47.2 kJ/mol (orange).

Figure 10. Distribution of the total binding energy of the first layer methylamine molecules (bottom panel), as well as its contributions coming from the interaction with the other methylamine molecules in the system (middle panel) and with the ice phase (top panel), as obtained at the surface of amorphous ice at selected chemical potential values at (a) 150 K, (b) 100 K, and (c) 50 K.

Figure 11. Distribution of the binding energy contribution coming from the interaction with the ice phase, as obtained for the methylamine molecules that are dissolved in the bulk amorphous ice phase at selected chemical potential values at 200 K (top panel), 150 K (second panel), 100 K (third panel), 50 K (fourth panel), and 20 K (bottom panel).

Figure 1

Horváth et al.

μ = -47.9 kJ/mol

μ = -39.6 kJ/mol

T = 20 K

μ = -32.1 kJ/mol

μ = -28.8 kJ/mol
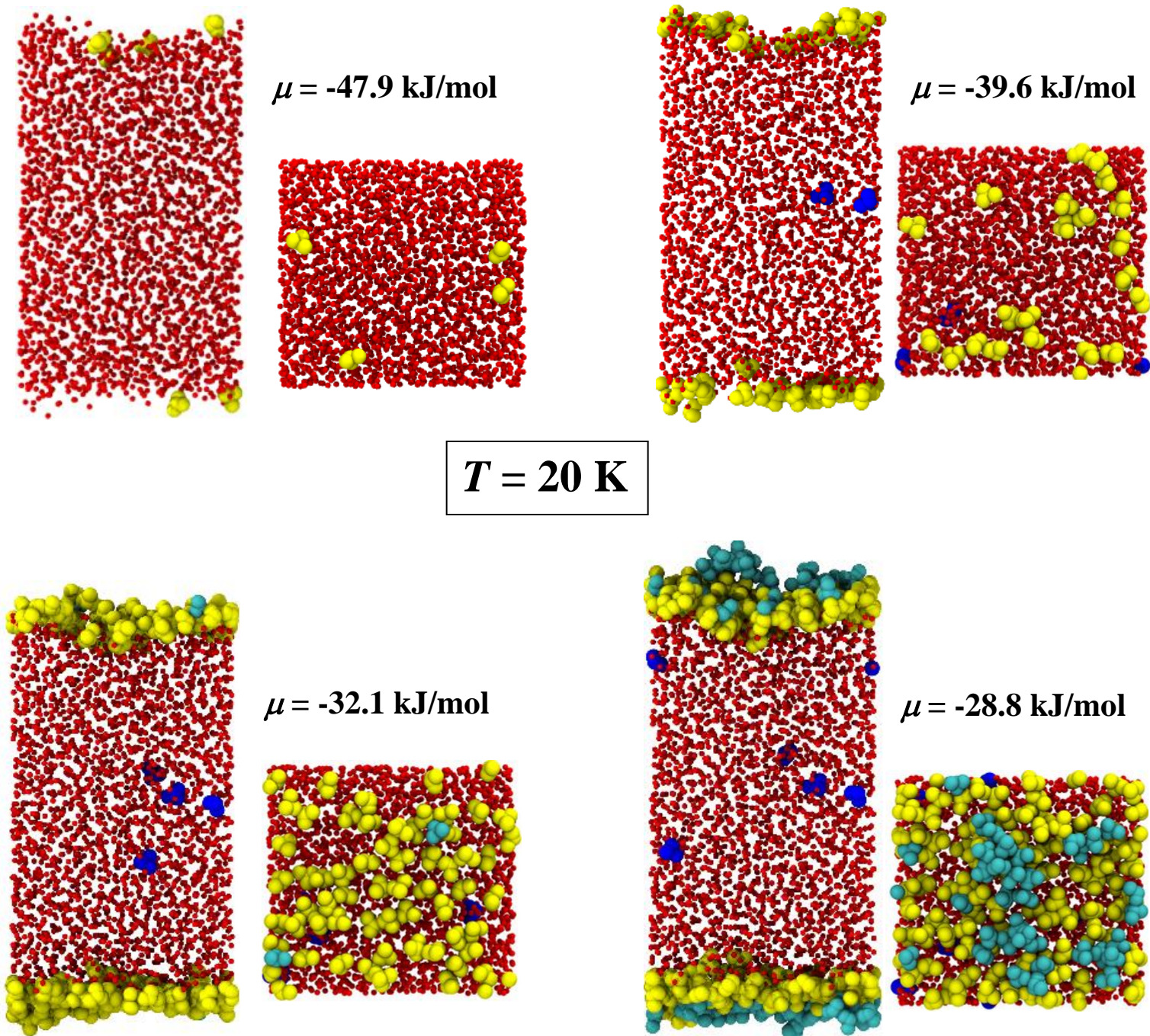
Figure 2
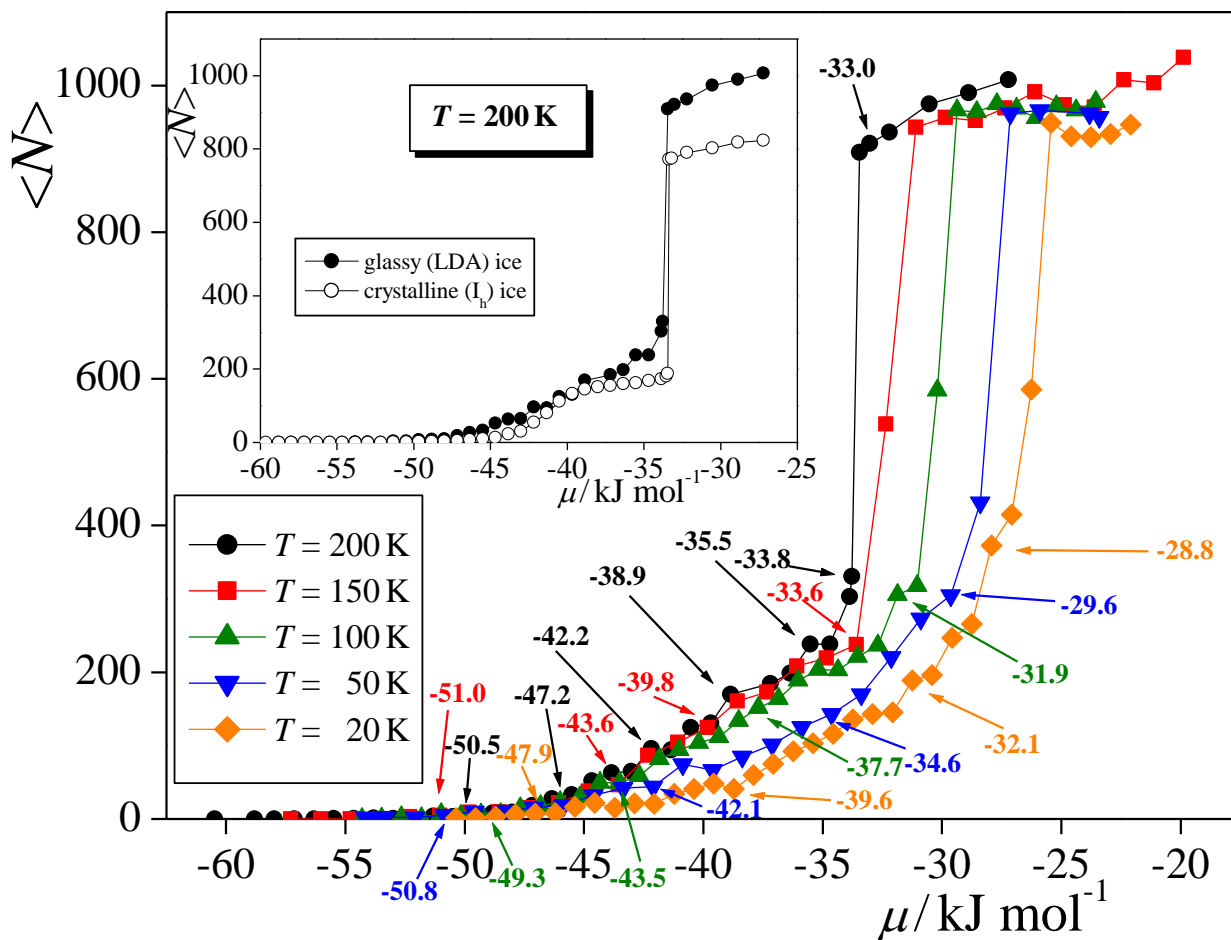
Horváth et al.
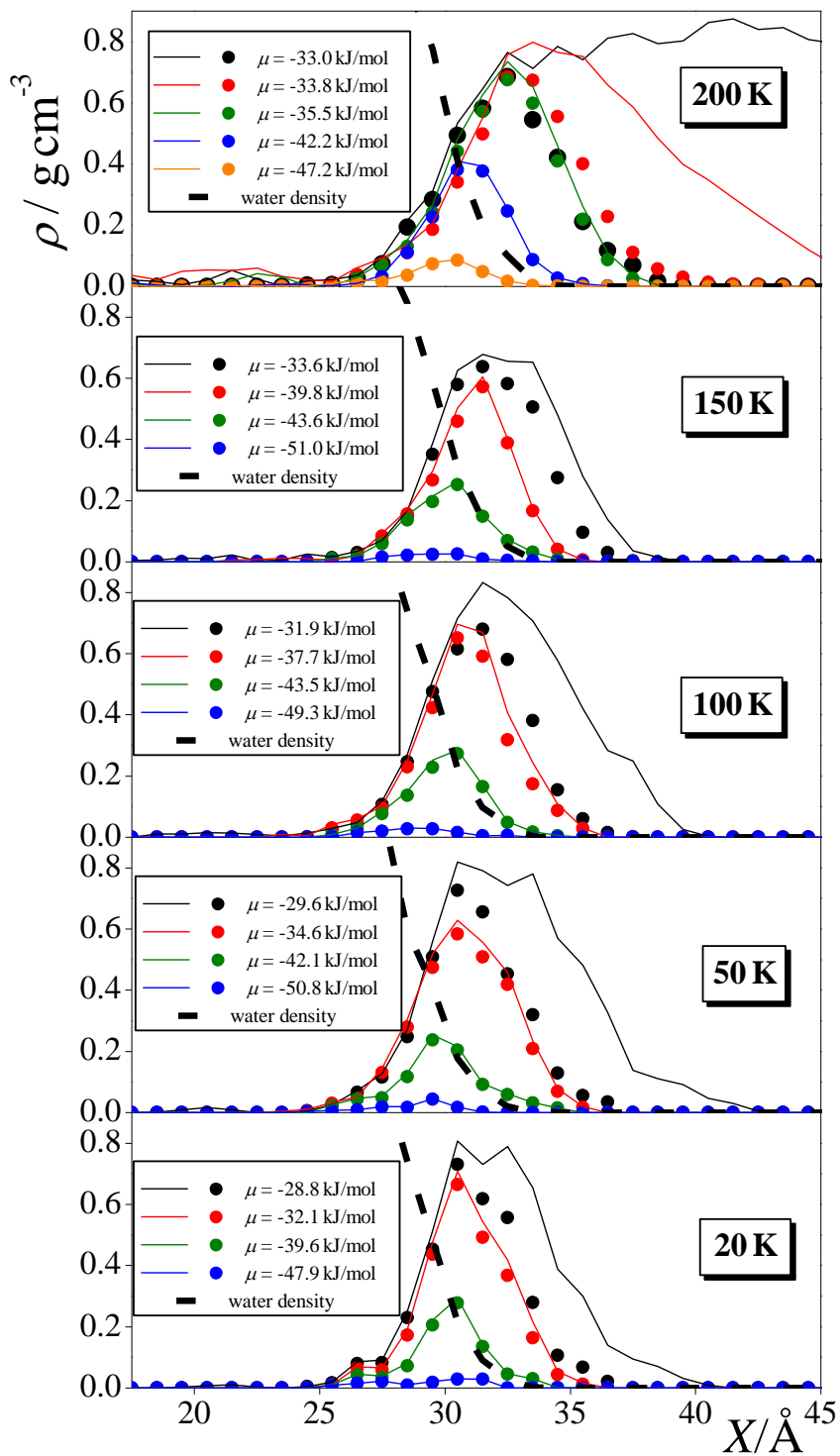
Figure 3

Horváth et al.
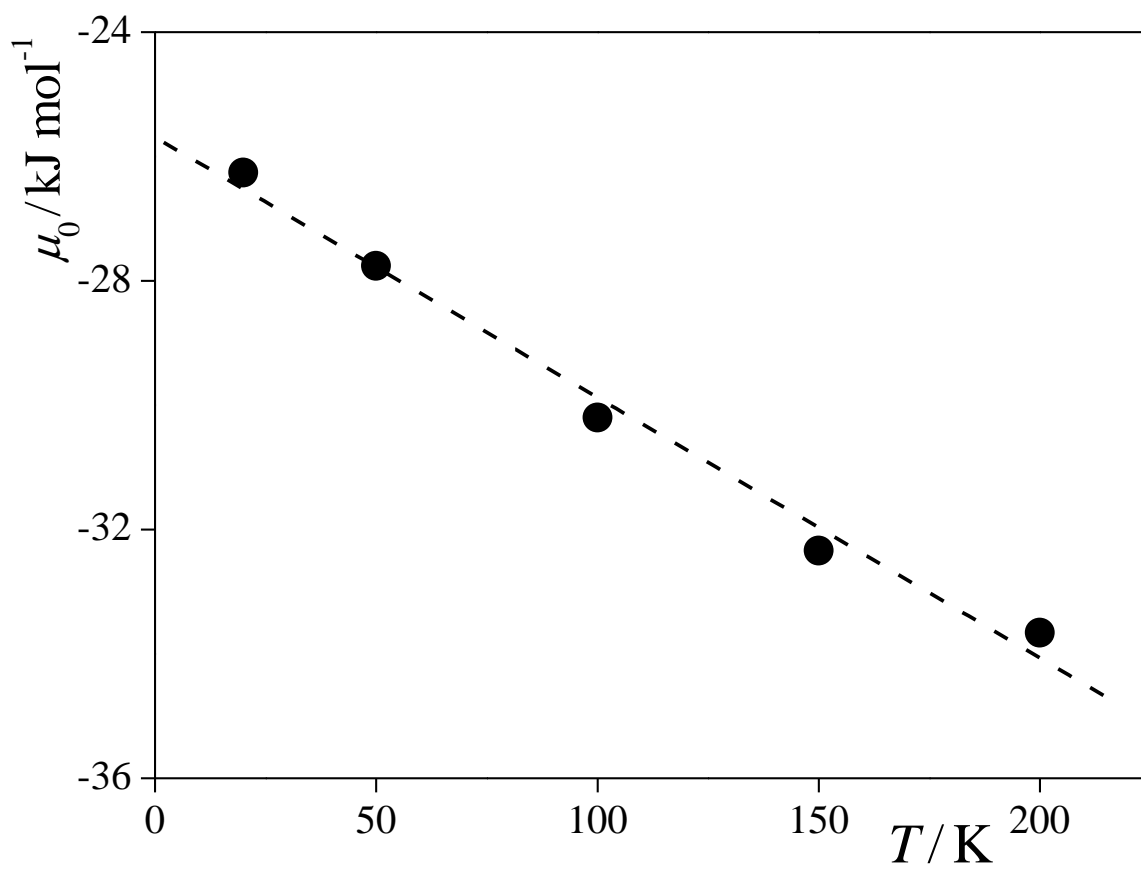
Figure 4

Horváth et al.
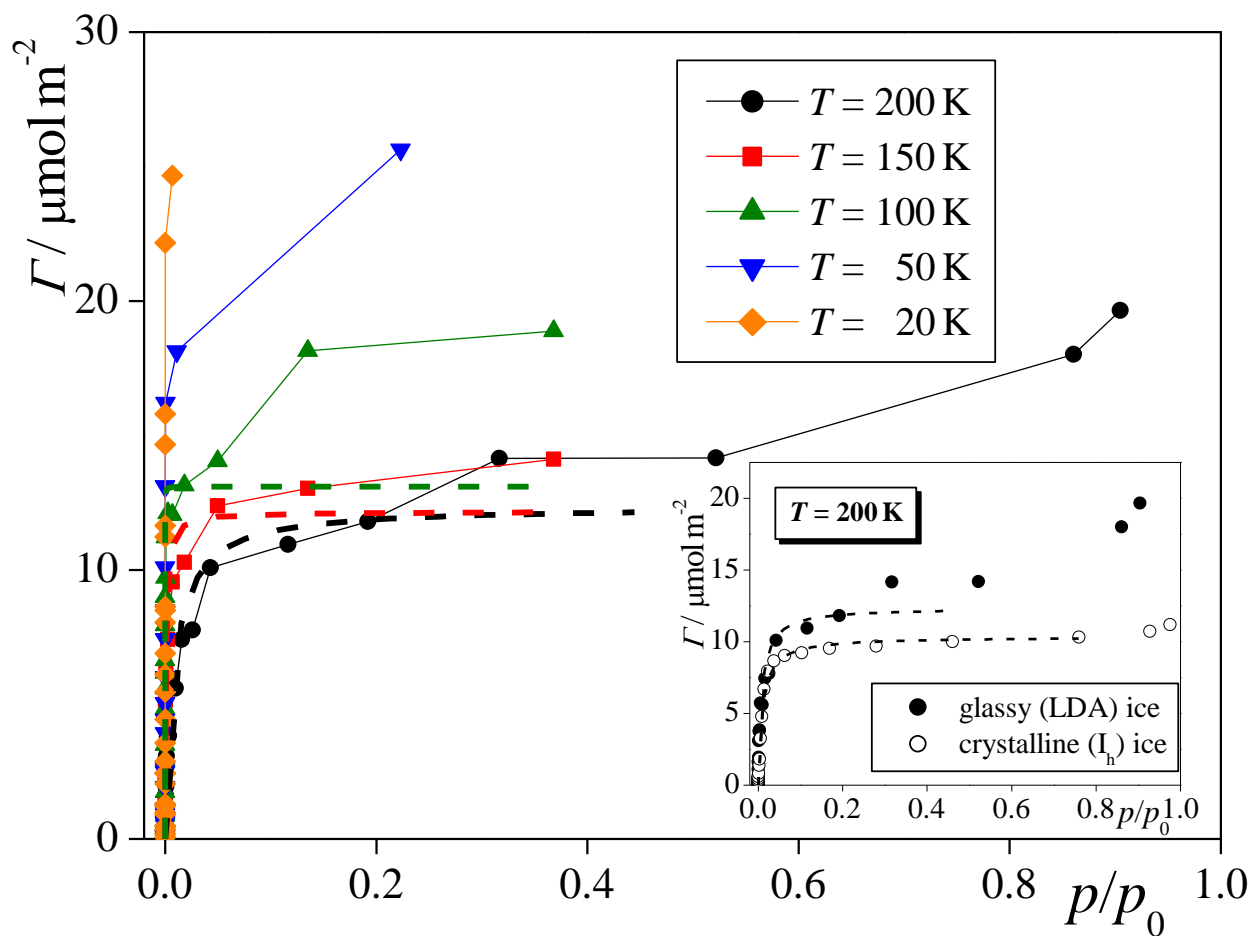
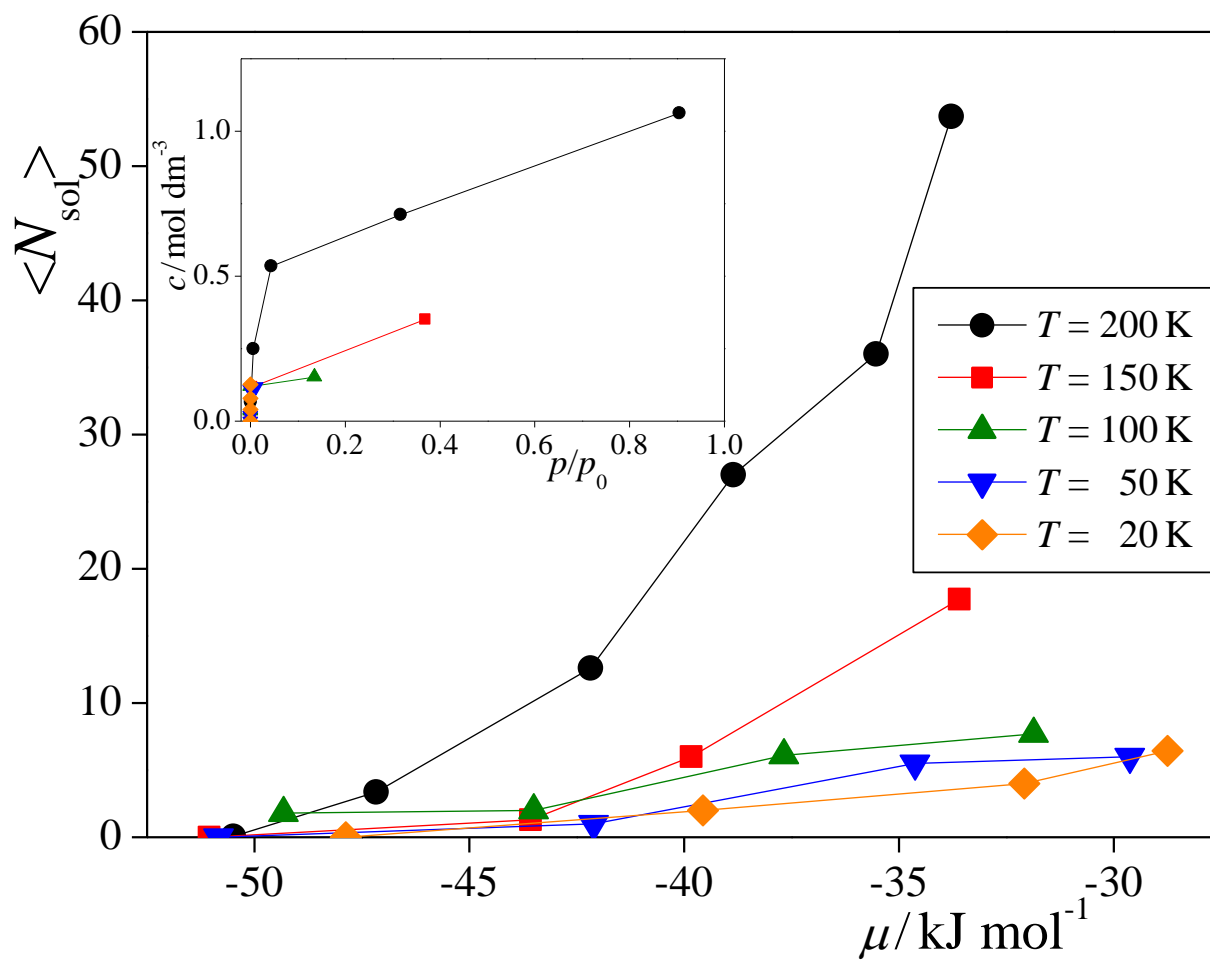Figure 5

Horváth et al.

Figure 6
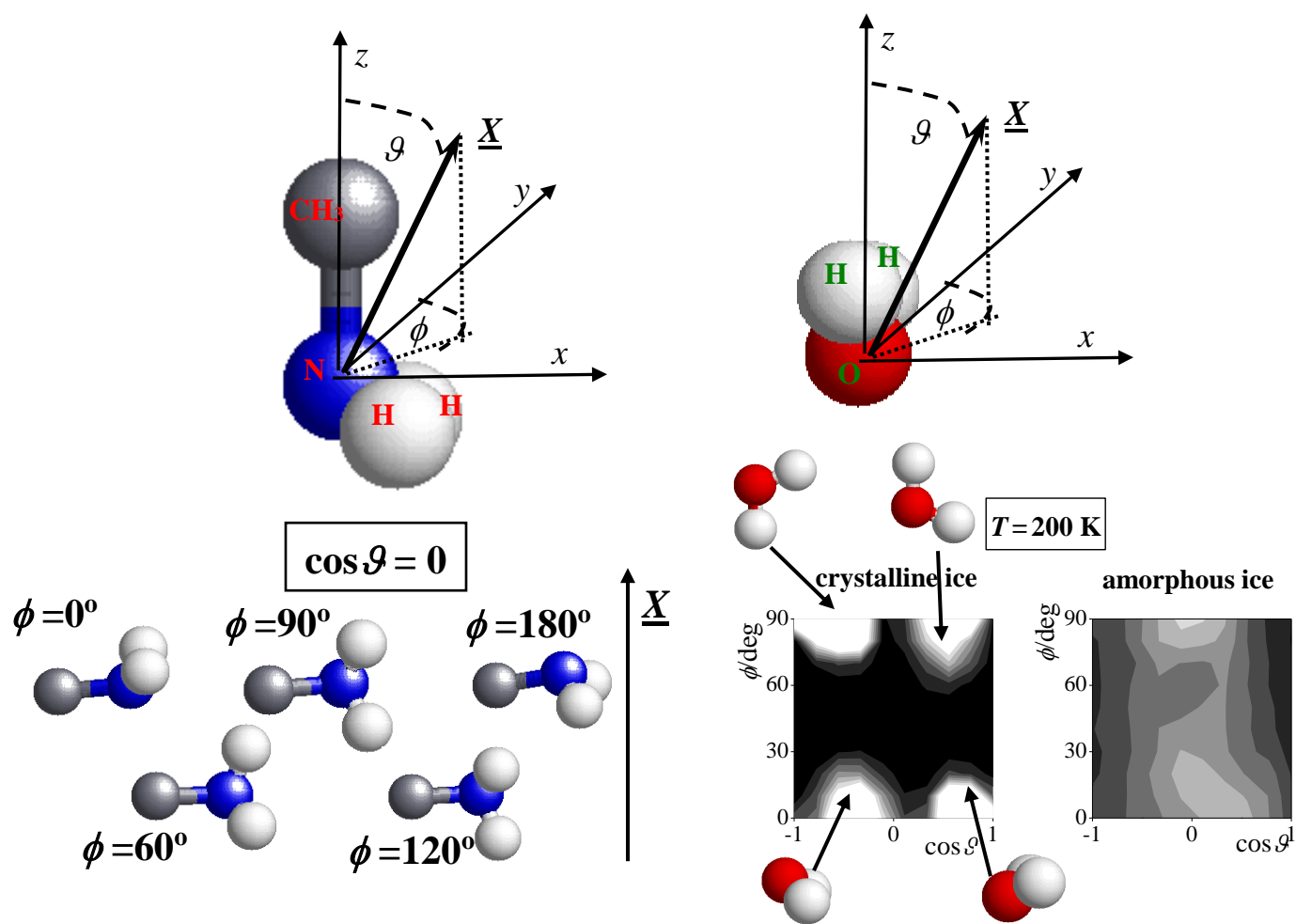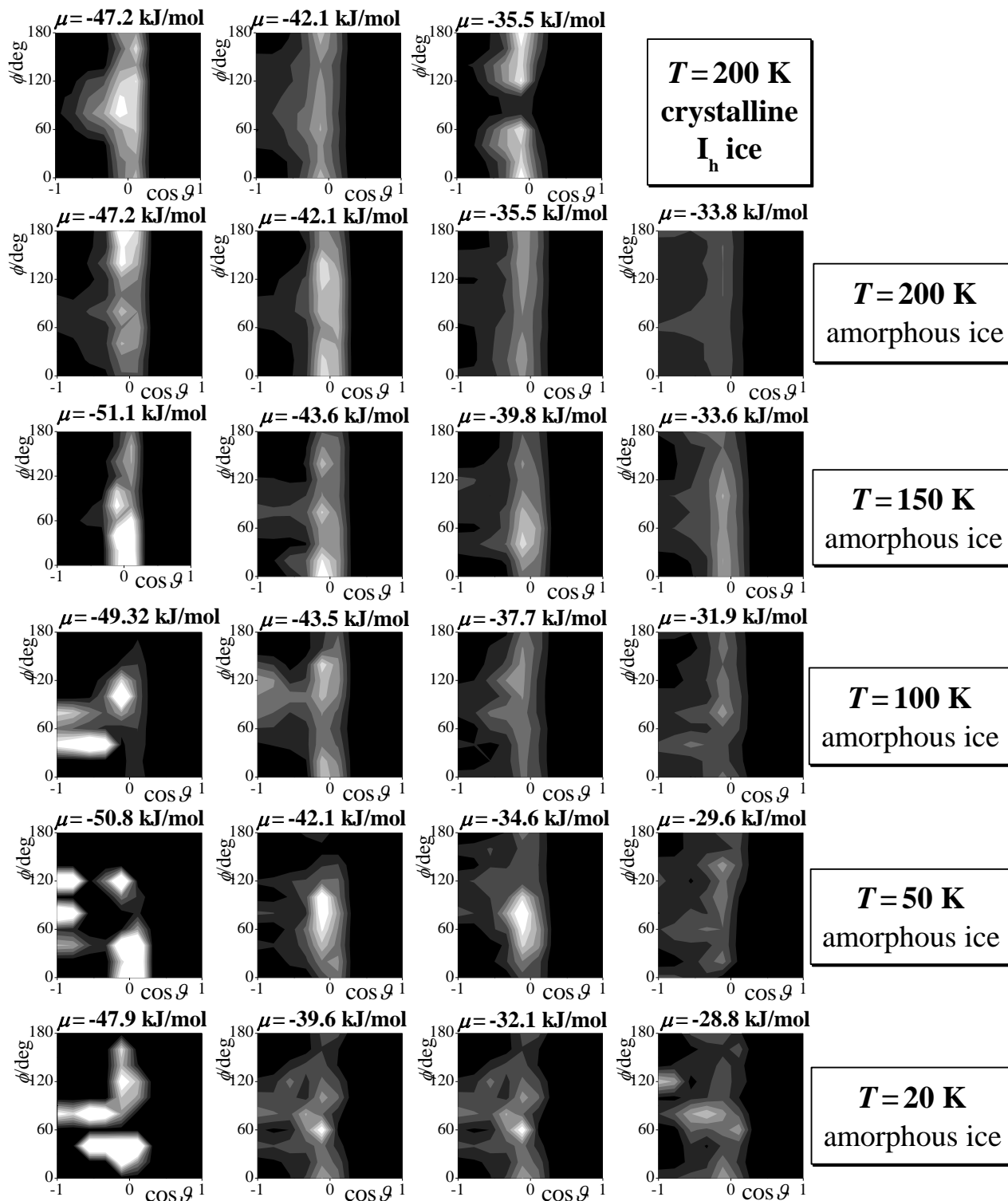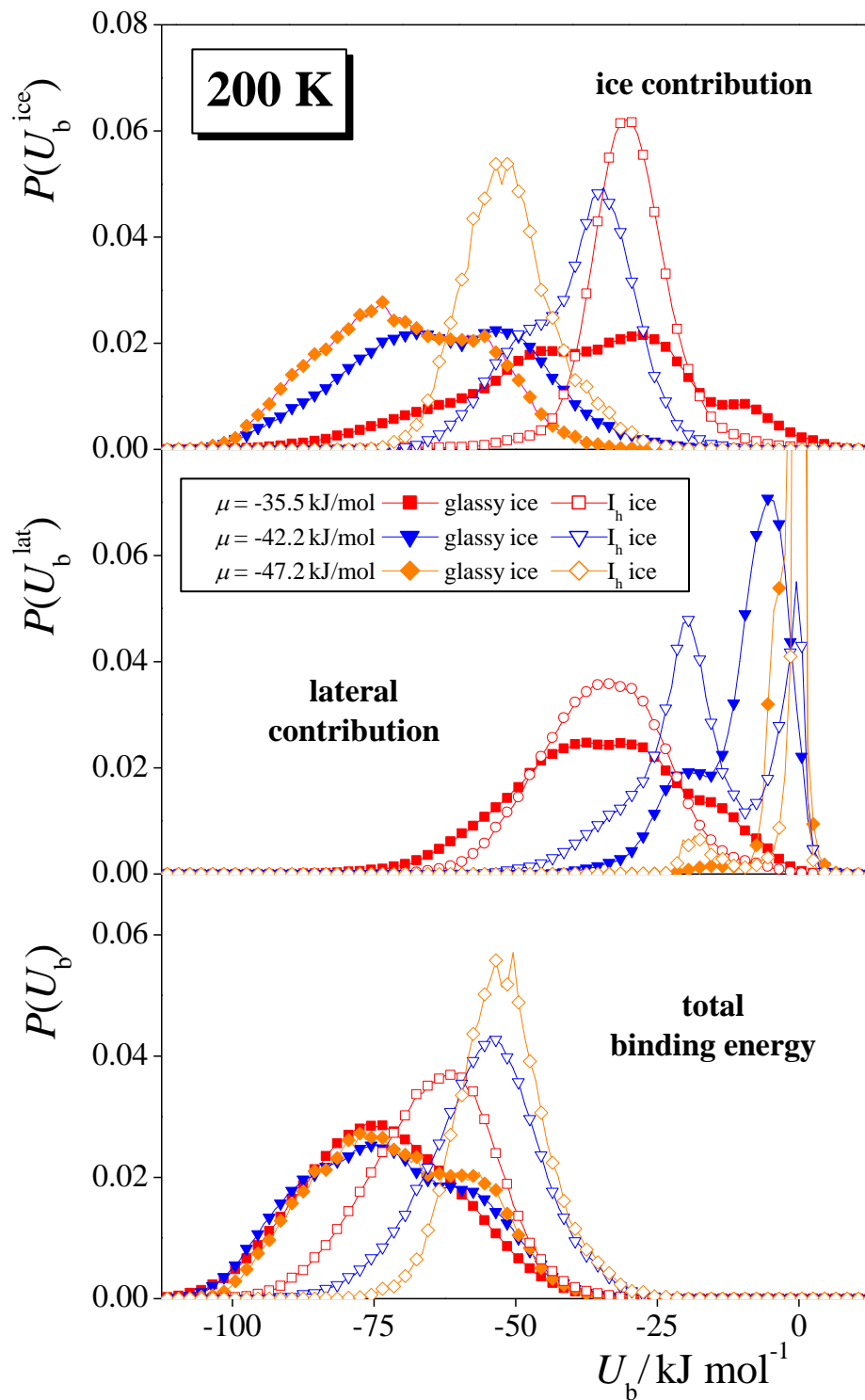
Horváth et al.

Figure 7

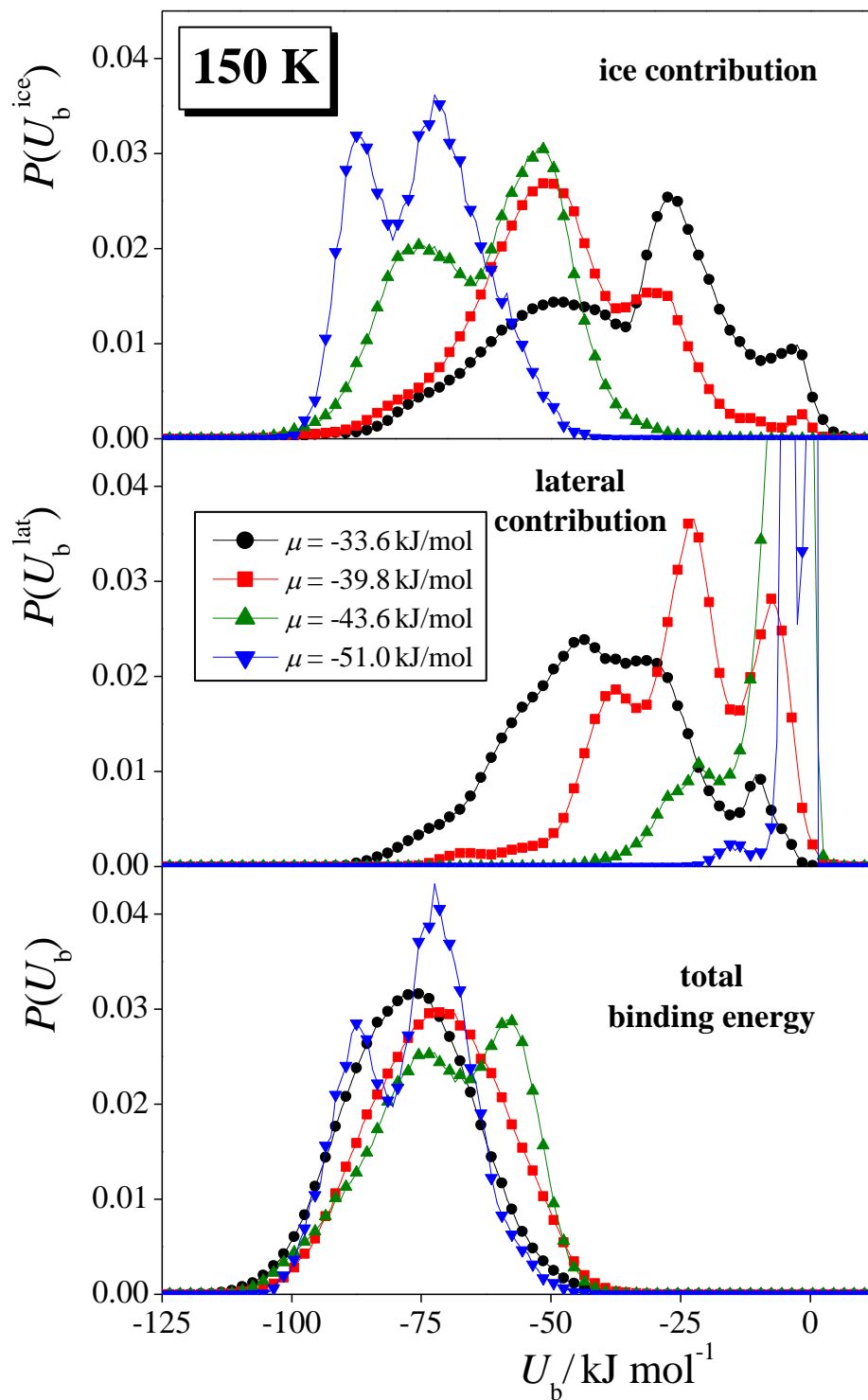**Horváth et al.**

$\cos\vartheta = 0$

Figure 8

Horváth et al.

41

Figure 9

Horváth et al.

Figure 10.a

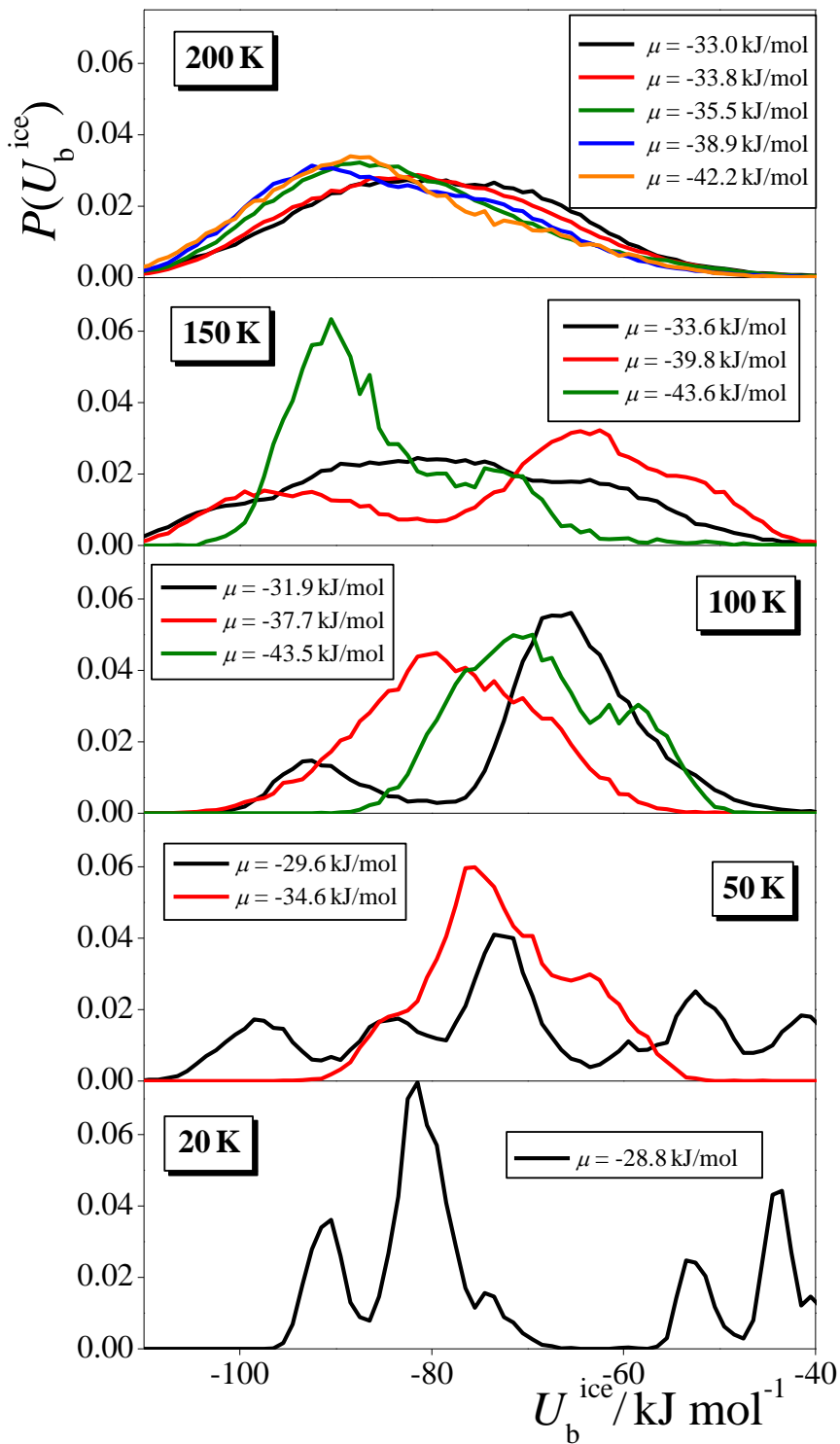Horváth et al.

Figure 10.b

Horváth et al.
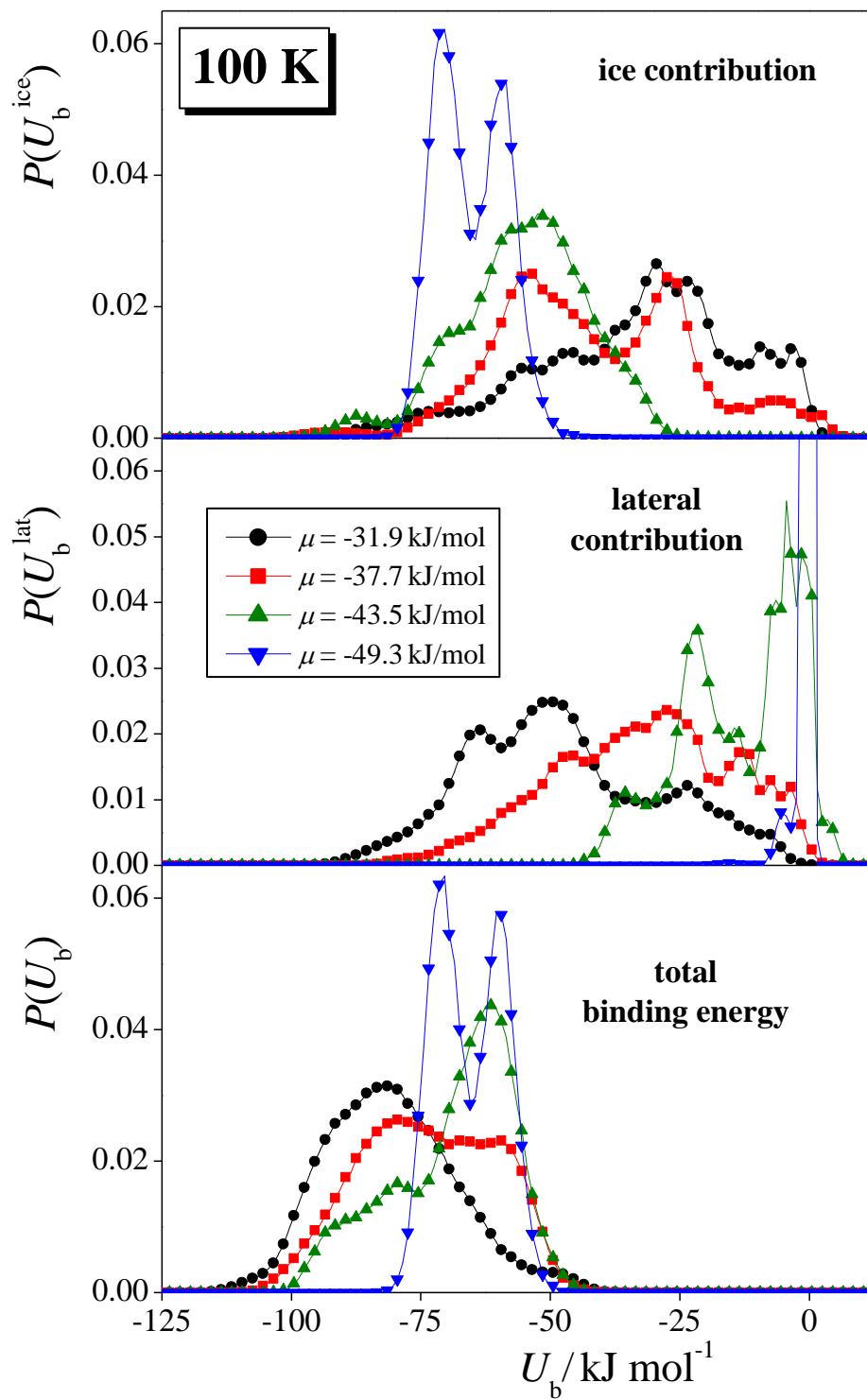
Figure 10.c

Horváth et al.
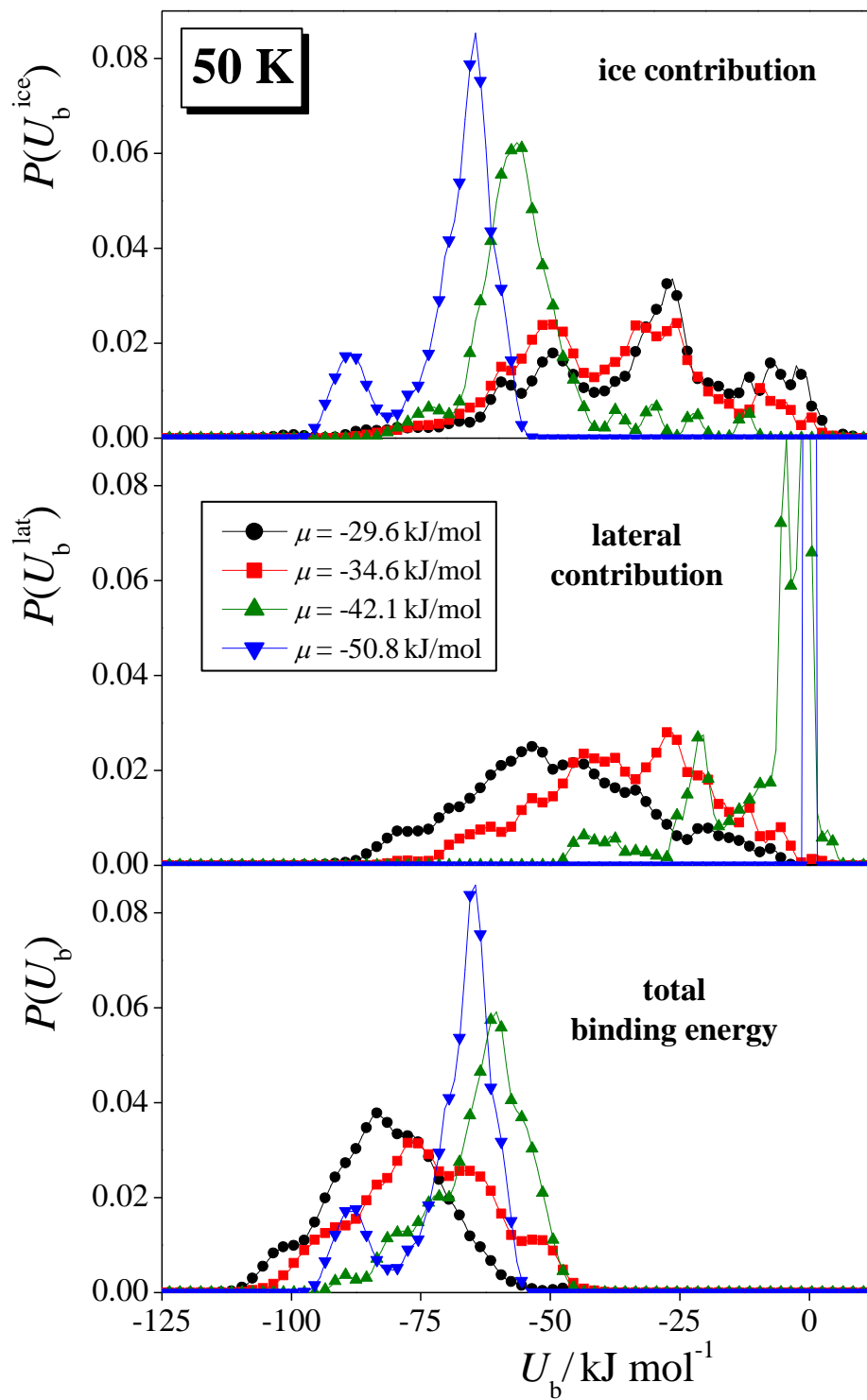
Figure 11

Horváth et al.

TOC Graphics: